IEEE Access
Multidisciplinary | Rapid Review | Open Access Journal

Received November 30, 2020, accepted December 10, 2020, date of publication December 15, 2020,
date of current version December 31, 2020.

Digital Object Identifier 10.1109/ACCESS.2020.3045045

Estimation and Tracking for Millimeter Wave MIMO Systems Under Phase Noise Problem

OSAMA S. FARAGALLAH[1], HALA S. EL-SAYED[2], AND MOHAMED G. EL-MASHED[3]
[1]Department of Information Technology, College of Computers and Information Technology, Taif University, Taif 21944, Saudi Arabia
[2]Department of Electrical Engineering, Faculty of Engineering, Menoufia University, Shebin El-Kom 32511, Egypt
[3]Department of Electronics and Electrical Communications, Faculty of Electronic Engineering, Menoufia University, Menouf 32952, Egypt

Corresponding author: Osama S. Faragallah (o.salah@tu.edu.sa and osam_sal@yahoo.com)

This work was supported by the Deanship of Scientific Research, Taif University Researchers Supporting Project number (TURSP-2020/08), Taif University, Taif, Saudi Arabia.

ABSTRACT Millimeter wave (mmWave) system is a key technology for the fifth generation (5G). Precoding techniques can be applied in the radio frequency (RF) stage to achieve spatial multiplexing gain. Studying the problems of hardware imperfections in the RF stage for mmWave communication system is very important because it can affect the transmitted signals and overall system performance. In this article, mmWave MIMO system under phase noise problem is proposed. In addition, an optimization problem for the design of hybrid precoder under phase noise is formulated. An alternating minimization algorithm using manifold optimization is proposed to close the performance of the fully digital precoder. A realistic power consumption model is considered. To estimate the mmWave channel parameters and to track the phase noise parameters, a Bayesian Cramér-Rao lower bounds (BCRLBs), Kalman filter, least square (LS) and maximum a posterior (MAP) algorithms are proposed. Furthermore, the proposed system with ideal hardware mmWave system is compared with non-ideal system under amplified thermal noise and residual additive transceiver hardware impairments. Spectral efficiencies (SEs) of the proposed system are provided with different scenarios. The analytical and simulation tests show that the influence of phase noise problem may decrease SE performance, especially at higher phase noise.

INDEX TERMS MmWave, hardware imperfections, BCRLBs MAP, LS and SE.

I. INTRODUCTION

Recently, the rapid development of mobile communications technology and the proliferation of integrated communications services have almost filled the low frequency radio band, which needs a rapid transfer rate. The mmWave communication is considered as a promised technology to empower the fifth generation (5G) networks, providing multiple gigabits per second for users. It has several enforcements in processing internet of things (IoT), business and wireless fusion networks, and high communications mission [1]. The mm-wave spectrum covers the 30 - 300 GHz frequency range, ten times higher than the current range of existing radio access technology (RAT) for less than 6 GHz vehicles [2], [3]. With the mmWave range in the extremely high frequency (EHF) range, large channels can be used for communication. These broad channels when simplified with better modulation and coding scheme (MCS), beamforming, and MIMO schemes can help in reducing distraction, enhancing spectral reuse, and allowing higher data quality support. Efficient bandwidth utilization is possible by enabling device-to-device (D2D) connectivity to next-generation networks. Using D2D connectivity in mmWave mobile networks, many direct corresponding links can be supported, which has led to improved network capacity.

The associate editor coordinating the review of this manuscript and approving it for publication was Zhenzhou Tang.

A. PRIOR WORK

The mmWave spectrum is large, which allows us to achieve high data rates. Large antenna arrays are employed at both mobile stations (MSs) and base station (BS) because of high path loss in the mmWave. This can also increase distance of communication links, can increase signal power and can achieve high quality links [4]–[9]. The challenge of the mmWave systems is the higher atmospheric absorption and pathloss. These challenging can be solved by using large antenna arrays for highly directional signaling. However,

application of directional beams can vary the features of the wireless communication systems [5]. These directional beams are affected by blockages and obstacles [7]. The performance of mmWave network systems is degraded by thermal noise (i.e., noise limited region) due to high attenuation, high bandwidth and highly narrow beams. In the interference-limited region, interference can degrade the performance of mmWave systems, which depends on probability of the transmission, obstacles density and beamwidth. Unlike classical wireless network systems, mmWave systems can transfer from the region of noise limited to interference limited or intermediate behavior between two regions [8]. The region in which mmWave systems are performed highly, can affects the strategies of resource allocation and the design of medium access control layer [9].

Massive MIMO systems can give high SEs, but this technology faces problems due to hardware imperfections. Another problem is the effects of channel aging and channel estimation, particularly at high mobility environments. These problems must be addressed to enhance system performance. The authors in [10] studied both the single-carrier frequency domain processing (SC-FDP) and the orthogonal frequency division multiplexing (OFDM) under these problems, which show that these problems can degrade system performance.

In [11], lens antenna arrays are employed in mmWave massive MIMO systems can decrease the number of power-hungry RF chains. However, works on this system have not studied the problem of power leakage in the channels, which decrease the system sum-rate and signal to noise ratio (SNR). To overcome the power leakage problem, a beam aligning precoding technique is introduced; each RF chain can choose many beams to collect the leakage power. Then, precoding technique with phase shifter network is built to adjust the channel gains of beams in the user direction with maximizing the signal-to-noise ratio. This technique can give optimal sum-rate performance and higher energy efficiency (EE).

The authors in [12] studied an analytical mmWave ad hoc network to calculate the distribution of interference-to-noise ratio. A narrowband channel model and a Poisson Point Process (PPP) distribution are considered for the transmitter positions. Large antenna arrays are employed to obtain line of sight/none line of sight directions and directional beamforming. Results showed that the interference power is higher than the noise power at high traffic of a network. As a result, the design of ad hoc mmWave network is required to deal with the problem of interference and obtain gigabit speeds.

Practically, hardware imperfections (i.e., impairments) from the RF chains should be considered in the design of mmWave systems. Hardware imperfections arise from low quality devices, amplifier, non-linearities and mutual coupling between antenna ports. It can cause many problems such as quantization errors, phase noise, inphase/quadrature imbalance, power losses and nonlinear power amplifier [13]–[19].

In [20], [21], authors measure the effect of hardware imperfections on the communication systems. The problem of inphase/quadrature imbalance may cause rotating the desired constellation phase and attenuating the amplitude. Also, the non-linear HPAs problem can cause constellation position distort in addition to an additive Gaussian noise. Some compensation algorithms are studied to reduce the impact of hardware imperfections. Hardware imperfections may result in a negative effect on the performance of the system, especially in high data rate [20], [21]. Studies in information theory have illustrated that hardware imperfections can affect the capacity of communication systems with multiple antennas [20]. Most of mmWave systems studies assume the hypothesis of ideal hardware devices.

These hardware imperfections can be compensated partially by compensation or pre-distortion methods, but there is always a remaining distortion that is not estimated and compensated [32]. The remaining distortion can reduce the channel estimation performance and can damage the training pilots. However, there are few studies to illustrate the hardware imperfections in mmWave systems. The authors in [13] studied the channel estimation algorithm for mmWave massive MIMO systems under ideal hardware devices. In [14], the channel estimation algorithm for massive MIMO systems is studied in the case of hardware imperfections, which did not study for mmWave systems.

The authors in [22] studied three sources of hardware imperfections, which are residual impairments, multiplicative impairments and thermal noise. The residual impairments can degrade the performance of the downlink transmissions than in uplink transmissions. In [23], massive MIMO is illustrated in the case of multiplicative impairments and the results showed that system degradation due to mobility of the user is increased with multiplicative impairments. The most motivation of the studies is done on the mmWave systems performance. For more realistic scenarios, it is essential to study the hardware imperfections for mmWave systems. The authors on [24] study the impact of residual impairments in mmWave systems using OFDM waveforms.

Many studies are concentrated on the design of precoder and how to reduce its complexity [25]–[28]. Precoding/beamforming schemes based on large-scale chemical composition can allow adequate advantages for overcoming free space losses and create enough SNR communications. For large MIMO configurations operating at mmWave frequencies, the transmitting antennas number can be high, so a fully digital configuration that allows high frequency replication benefits needs a separate RF for each antenna, which is impossible because of high power and extra problematic power [29]–[32]. For large scale MIMO construction, the hybrid precoding structure constructed with the high RF precoder and low cost digital precoder proposed in [30] is receiving much attention. There are two kinds of hybrid precoding frames that are mostly investigated in the literature; 1) fully connected scheme in which whole antennas are linked to each RF chain with a phase shifter, and b) lowly connected

scheme in which some of antennas are connected to the RF series.

The transceiver designs for hybrid sub-array architecture and hybrid MIMO architectures with compressive sensing estimation studied in [33] and [34], respectively. Although demonstrated that these transceiver design in mmWave systems can give high SE, numerous studies consider ideal hardware. Practically, mmWave systems have hardware imperfections, thus degrading their performance.

In [35], beamforming mmWave MIMO architectures under residual hardware impairments is studied. The hardware impairments are modeled as additional distortion noise. Results showed that there is a ceiling effect in the capacity performance, meaning that it cannot increase the system capacity with the higher signal-to-noise ratio.

The authors in [36] studied the problems of hardware imperfections, which are non-linear power amplifiers, analog-to-digital converter resolution and phase noise. The analysis is performed on OFDM and SC-FDP for mmWave communications. From results single-carrier frequency domain equalization is robust against analog-to-digital converter resolution and non-linear power amplifiers than orthogonal frequency division multiplexing. The channel coding is illustrated to mitigate the less robustness of orthogonal frequency division multiplexing to a large extent.

The authors in [37] studied hardware aspects at 60 GHz for the wireless personal area networks. Hardware problems such as non-linear power amplifiers and phase noise are considered. The OFDM and SC-FDP systems over an AWGN propagation channel beneath RF impairments using programming tools at 60 GHz are studied in [38]. Similar studies and comparisons are introduced for an indoor wireless personal area networks environment in [39]. Also, an outdoor mmWave case with 3D channel model [40] using a sectorized beamforming method [41] is illustrated.

The channel estimation problem is explained in [42] for mmWave systems in the case of transmitter hardware impairments. Results show that the performance of the classical pilots-based channel estimation method is degraded due to hardware impairments, which can damage training pilots. Using the property of mmWave channel sparsity, the authors in [42] studied Bayesian compressive sensing for channel estimation, which give better performance compared to the orthogonal matching pursuit algorithm. The impact of path loss can be compensated using hybrid precoding schemes [43]. There is a challenge task in the compensation of the effects of phase noise in mmWave systems.

Phase noise problem can give high frequency shifts and can rapidly vary in time. Many algorithms are employed to give constant frequency offsets, but these algorithms cannot do the same job in the case of higher phase noise [43]. This can lead to apply the multicarrier modulation for mmWave systems. At higher frequencies 72 GHz, the RF hardware imperfections will be amplified over the effects at classical cellular frequencies. At the mmWave band, one dominant source of hardware imperfections is the increased phase noise [44]. This problem can be large enough to need tracking from one data symbols to another. The authors in [45] illustrated the mmWave system in the case of phase noise, which it is created by the local oscillators. Due to large phase noise, there is unknown phase value, which varies from one block to another in block-processing systems. Blind phase noise compensation technique is addressed for the tracking of phase noise in single-carrier communication system, which brings better performance.

In [46], mmWave MIMO system under residual transceiver hardware impairments is addressed. Also, three sources (i.e., residual impairments, multiplicative impairments and thermal noise) is studied. The SE is deduced to demonstrate the effect of these problems on system performance. There is degradation in the SE performance and phase noise is the dominant impact. The hardware imperfections are a challenge task in the design of mmWave transceivers. Thus, the paper goal is to study the effectiveness of hardware imperfections on mmWave systems with hybrid precoding and how to mitigate it by proposing compensation and tracking algorithms. A summary of related works are listed in Table 1.

B. CONTRIBUTIONS

We illustrate a comprehensive analysis on the mmWave system performance by calculating the spectral efficiency. It facilities the ability of determine the impact of hardware imperfections at any SNR value. The main contributions are:

- MmWave MIMO system under hardware imperfections is proposed.
- A realistic power consumption model is demonstrated.
- Formulate an optimization problem for designing analog and digital precoders.
- An alternating minimization algorithm is proposed to solve the optimization problem.
- Propose BCRLBs, Kalman filter, LS and MAP algorithms for tracking the phase noise parameters.
- Comparison between the traditional mmWave system and the proposed mmWave system is provided in terms of SE.

C. ORGANIZATION

The paper remainder is arranged as follows. Section II illustrates phase noise problem along with its model. Section III shows the proposed mmWave cellular system under hardware imperfections. Section IV explains the design of hybrid precoder and combiner. The proposed channel estimation techniques is derived in Section V. Section VI explains the tracking of phase noise. Section VII shows the model of power consumption. Simulation tests and concluded remarks are explored in Sections VIII and IX.

II. PHASE NOISE PROBLEM AND ITS MODEL

The parameter that describes the behavior of phase noise is illustrated in this section. Phase noise problem is the instabilities of the phase values in communication systems. It can degrade the performance of communication systems [23]–[26]. It can cause signal constellation rotation

TABLE 1. Comparison of proposed scheme with respect to related works.

Ref.	Problem	System	Solution	Studies
[8]	Power noise problem and interference	mmWave systems	NO	SE
[10]	Channel aging and channel estimation	OFDM and SC-FDP	NO	SE
[11]	Power leakage problem	mmWave massive MIMO system	Beam aligning precoding technique	Sum-rate and and SNR
[13]	Ideal hardware	mmWave massive MIMO systems	Compressed sensing	SE
[32]	Hardware imperfections	Massive MIMO system	NO	Energy efficiency
[17]	Nonlinear amplifier and phase noise	m-QAM-OFDM system	NO	BER
[20]-[21]	Inphase/quadrature imbalance and non-linear high power amplifier	Communication system	Compensation algorithms	BER
[22]-[23]	Residual impairments, multiplicative impairments and thermal noise	Massive MIMO system	NO	BER
[24]	Residual impairments	mmWave system	NO	SE
[33]-[34]	Ideal hardware	Hybrid MIMO architectures	NO	SE
[35]	Additional distortion noise	Beamforming mmWave MIMO	NO	Capacity
[36]	Non-linear power amplifiers, ADC resolution and phase noise	OFDM mmWave communications	Channel coding	SE
[37], [39]	Non-linear power amplifiers and phase noise	Wireless personal area networks	NO	BER
[42]	Hardware impairments	mmWave system	Bayesian compressive sensing scheme	SE
[43]-[44]	Phase noise	mmWave system	NO	SE
[45]	Phase noise	Single carrier communication	. Blind phase noise compensation	SE
[46]	Residual impairments, multiplicative impairments and thermal noise	mmWave MIMO	NO	SE
Proposed Scheme	Phase Noise	mmWave cellular systems	BCRLBs, Kalman filter, LS and MAP	SE

from symbol to another symbol. Consider the transmitted signal x is influenced by a fading channel h and an additive noise v. The received signal in cell i at a given channel uses $t \in \{1, \ldots, T\}$ of RF transceiver system under phase noise can be expressed as:

$$\mathbf{y}_i(t) = \mathbf{D}_{\phi_i(t)} \sum_{l=1}^{L} \mathbf{H}_{il} \mathbf{x}_l(t) + v_i(t), \tag{1}$$

where $\mathbf{D}_{\phi_i(t)}$ is the phase noise, which consists of phase drifts as:

$$\mathbf{D}_{\phi_i(t)} \triangleq \text{diag}\left(e^{j\theta_1(t)}, \ldots, e^{j\theta_N(t)}\right). \tag{2}$$

where j is the imaginary unit and θ_n is the phase-drift of nth receive antenna. The variable $\theta_n(t)$ in local oscillators (LOs) is considered as a Wiener process $\theta_n(t) \sim N(\theta_n(t-1), \delta)$, which equivalent to the previous realization $\theta_n(t-1)$ in addition to Gaussian innovation of variance δ [20]. The phase drifts are autonomous between the antennas and correlated. In distributed arrays of separated LOs, the phase drifts are autonomous and phase-drifts variance δ are equal. The distributed array is assumed in the proposed mm-wave system. The variance δ is one of the important parameters to analyze this problem.

III. THE PROPOSED mmWave MIMO SYSTEM UNDER HARDWARE IMPERFECTION

A. SYSTEM BLOCK DIAGRAM AND SIGNAL MODEL

In this section, we propose a mmWave MIMO system with the existence of phase noise problem as illustrated in Fig. 1.

The BS has N_t antennas and L_t RF chains. It can communicate with a MS, which has N_r antennas and L_r RF chains.

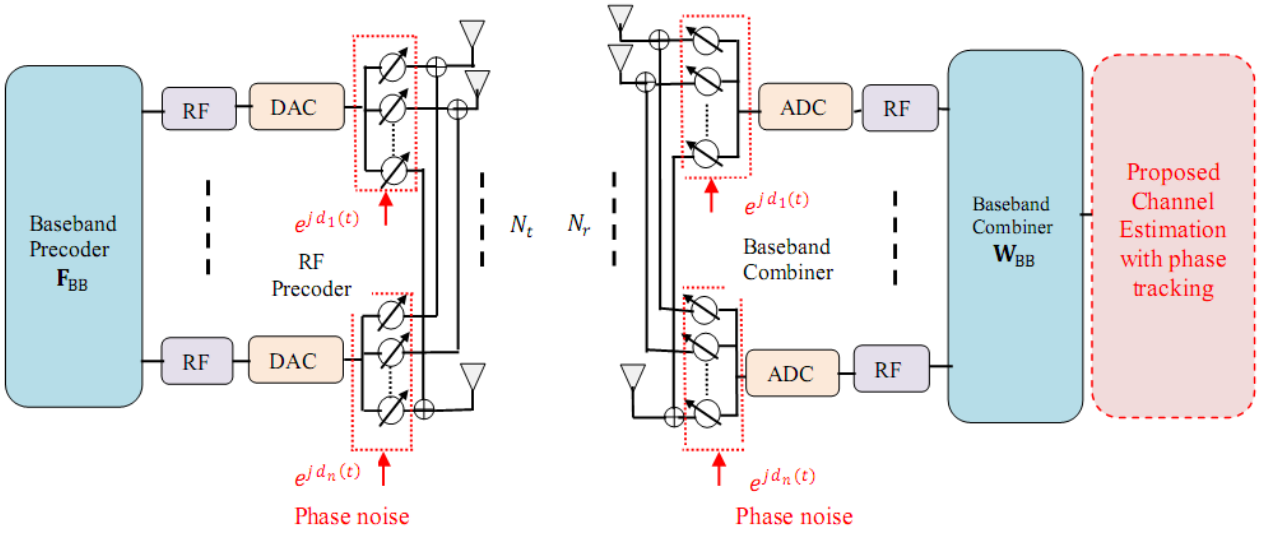

FIGURE 1. The proposed mmWave cellular system model under hardware phase noise problem.

The information N_s is transferred from BS to MS considering $N_s \leq L_t \leq N_t$ and $N_s \leq L_r \leq N_r$ as in practical case. The BS uses $N_s \times L_t$ hybrid precoder $\mathbf{F}$ to the input data $\mathbf{s} \in \mathbb{C}^{N_s \times 1}$ with $\mathbf{E}\left[\mathbf{s}\mathbf{s}^H\right] = \mathbf{I}$. The signal from BS is $\mathbf{Fs}$. Assume fully connected structure, where phase shifters at both transmitters and the receiver are connected with each antenna in the RF chains. The data are processed using the hybrid precoder $\mathbf{F} = \mathbf{F}_{\mathrm{BB}}\mathbf{F}_{\mathrm{RF}} \in \mathbb{C}^{N_s \times N_t}$. It consists of a baseband precoder $\mathbf{F}_{\mathrm{BB}} \in \mathbb{C}^{N_s \times L_t}$ and an RF precoder $\mathbf{F}_{\mathrm{RF}} \in \mathbb{C}^{N_t \times L_t}$.

At the receiving part, the signal is filtered with the hybrid $\mathbf{W} = \mathbf{W}_{\mathrm{BB}}\mathbf{W}_{\mathrm{RF}}$. It consists of a baseband combiner $\mathbf{W}_{\mathrm{BB}} \in \mathbb{C}^{N_s \times L_r}$ and an RF combiner $\mathbf{W}_{\mathrm{RF}} \in \mathbb{C}^{N_r \times L_r}$. The transmitted signal at time k is:

$$x(k) = \mathbf{H}\boldsymbol{\Theta}^{[t]}\mathbf{F}_{\mathrm{RF}}\mathbf{F}_{\mathrm{BB}}\mathbf{s}(k) + \mathbf{n}(k) \tag{3}$$

The baseband received signal vector, $\mathbf{y}(k) = \left[y_1(k), \ldots, y_{N_r}(k)\right]^T$ after combing process is:

$$\mathbf{y}(k) = \boldsymbol{\Theta}^{[r]}\mathbf{W}_{\mathrm{BB}}^H\mathbf{W}_{\mathrm{RF}}^H\mathbf{H}\boldsymbol{\Theta}^{[t]}\mathbf{F}_{\mathrm{RF}}\mathbf{F}_{\mathrm{BB}}\mathbf{s}(k) + \mathbf{W}_{\mathrm{BB}}^H\mathbf{W}_{\mathrm{RF}}^H\mathbf{n}(k) \tag{4}$$

The received signal in vector and matrix form can be written as:

$$\mathbf{y}(k) = \mathbf{W}_{\mathrm{BB}}^H\mathbf{W}_{\mathrm{RF}}^H\left(\mathbf{A} \odot \mathbf{e}^{j\mathbf{B}(\mathrm{n})}\right)\mathbf{F}_{\mathrm{RF}}\mathbf{F}_{\mathrm{BB}}\mathbf{s}(k) + \mathbf{W}_{\mathrm{BB}}^H\mathbf{W}_{\mathrm{RF}}^H\mathbf{n}(k) \tag{5}$$

Let $\mathbf{P}(\mathrm{n}) = \mathbf{A} \odot \mathbf{e}^{j\mathbf{B}(\mathrm{n})}$, then

$$\mathbf{y}(k) = \mathbf{W}_{\mathrm{BB}}^H\mathbf{W}_{\mathrm{RF}}^H\mathbf{P}(\mathrm{n})\,\mathbf{F}_{\mathrm{RF}}\mathbf{F}_{\mathrm{BB}}\mathbf{s}(k) + \mathbf{W}_{\mathrm{BB}}^H\mathbf{W}_{\mathrm{RF}}^H\mathbf{n}(k) \tag{6}$$

where

- $\mathbf{s}(k) \triangleq \left[s_1(k), \ldots, s_{N_t}(k)\right]^T$ with $s_{\mathrm{m}}(k)$ is the M-ary modulated signal transferred from mth antenna at time k;
- $\mathbf{F}_{\mathrm{BB}}$ is the $N_s \times L_t$ baseband precoder;
- $\mathbf{F}_{\mathrm{RF}}$ is the $N_t \times L_t$ RF precoder;
- $\mathbf{W}_{\mathrm{BB}}$ is the $N_s \times L_r$ baseband combiner;
- $\mathbf{W}_{\mathrm{RF}}$ is the $N_r \times L_r$ RF combiner;
- $\mathbf{H} \in \mathbb{C}^{N_r \times N_t}$ is the channel matrix with $\mathbb{E}\left[\|\mathbf{H}\|_F^2\right] = N_r N_t$;
- $\mathbf{n} \in \mathbb{C}^{N_r \times N_t}$ defines the noise vector with i.i.d $\mathcal{CN}\left(0, \sigma_n^2\right)$ elements;
- $\boldsymbol{\Theta}^{[r]}(k) \triangleq diag\left(e^{j\theta_1^{[r]}(k)}, \ldots, e^{j\theta_{N_r}^{[r]}(k)}\right)$ and $\boldsymbol{\Theta}^{[t]}(k) \triangleq \mathrm{diag}\left(e^{j\theta_1^{[t]}(k)}, \ldots, e^{j\theta_{N_t}^{[t]}(k)}\right)$ are the $N_r \times N_r$ and $N_t \times N_t$ diagonal matrices, respectively;
- $\theta_i^{[r]}(k)$ is the kth phase noise sample at the ith receive antenna;
- $\theta_j^{[t]}(k)$ is the kth phase noise sample at the jth transmit antenna;
- $\mathbf{A} \triangleq \left[\alpha_1, \ldots, \alpha_{N_r}\right]^T$ is the $N_r \times N_t$ channel gain matrix;
- $\mathbf{B}(\mathrm{n}) \triangleq \left[\beta_1(n), \ldots, \beta_{N_r}(n)\right]^T$ is the $N_r \times N_t$ phase shift matrix;
- $\alpha_{k,l} \triangleq \left|h_{k,l}\right|$ is the channel gain between lth and kth antenna for the transmitter and receiver, respectively;
- $\beta_{k,l}(n) \triangleq \theta_l^{[t]} + \theta_k^{[r]} + \angle h_{k,l}$ is the total phase shift.

The model of phase noise in the above equation can be represented as a Wiener process [49]–[52]. The phase noise $\theta_j^{[t]}(k)$ at the jth transmit antenna and $\theta_i^{[r]}(k)$ ith receive antenna, respectively is given by:

$$\theta_j^{[t]}(k) = \theta_j^{[t]}(k-1) + \Delta_l^{[t]}(k) \tag{7}$$

$$\theta_i^{[r]}(k) = \theta_i^{[r]}(k-1) + \Delta_l^{[r]}(k) \tag{8}$$

where $\Delta_l^{[t]}(k)$ and $\Delta_l^{[r]}(k)$ are the phase noise rate and it is considered Gaussian Process with $\Delta_l^{[t]}(k) \sim \mathcal{N}\left(0, \delta^2_{\Delta_l^{[t]}}\right)$ and $\Delta_l^{[r]}(k) \sim \mathcal{N}\left(0, \delta^2_{\Delta_l^{[r]}}\right)$, respectively.

The phase noise $\mathbf{B}(\mathrm{n})$ and the channel gains $\mathbf{A}$ are assumed to be unknown. The variations of $\mathbf{A}$ are slow compared to the

variations of $\boldsymbol{\Theta}$. So, the estimated data is used to estimate the values of $\mathbf{B}$ and $\mathbf{A}$.

B. CHANNEL MODEL

A clustered channel model (i.e., Saleh-Valenzuela model) characterizes the environment of mmWave propagation due to high free-space path loss. It applied for mmWave propagation system [47], [48]. The channel matrix $\mathbf{H}$ can be represented by:

$$\mathbf{H} = \sqrt{\frac{N_t N_r}{N_{cl} N_{ray}}} \sum_{i=1}^{N_{cl}} \sum_{l=1}^{N_{ray}} \boldsymbol{\alpha}_{il} \boldsymbol{R}_r \left(\boldsymbol{\phi}_{il}^r, \boldsymbol{\theta}_{il}^r\right) \boldsymbol{T}_t \left(\boldsymbol{\phi}_{il}^t, \boldsymbol{\theta}_{il}^t\right)^H \tag{9}$$

where N_{ray} and N_{cl} are the beams number and the clusters number in each cluster, respectively and $\boldsymbol{\alpha}_{il}$ is the lth ray gain for ith cluster. The parameter $\boldsymbol{\alpha}_{il}$ is independent and identically distributed, $\mathcal{CN}(0, \sigma_{\alpha,i}^2)$ and the normalization factor $\sum_{i=1}^{N_{cl}} \sigma_{\alpha,i}^2 = \hat{\gamma}$, satisfy $\mathbb{E}\left[\|\boldsymbol{H}\|_F^2\right] = N_t N_r$. The array response vectors for the receiver and the transmitter are $\boldsymbol{R}_r \left(\boldsymbol{\phi}_{il}^r, \boldsymbol{\theta}_{il}^r\right)$ and $\boldsymbol{T}_t \left(\boldsymbol{\phi}_{il}^t, \boldsymbol{\theta}_{il}^t\right)^H$, respectively. Also, the azimuth and elevation angles of arrival and departure are $\boldsymbol{\phi}_{il}^r, \boldsymbol{\phi}_{il}^t$ and $\boldsymbol{\theta}_{il}^r, \boldsymbol{\theta}_{il}^t$,respectively. Assuming that $\sqrt{N} \times \sqrt{N}$ uniform planar array antennas. The array response for the transmitter and the receiver, respectively are:

$$\boldsymbol{R}_r \left(\boldsymbol{\phi}_{il}^r, \boldsymbol{\theta}_{il}^r\right) = \frac{1}{\sqrt{N}} \begin{bmatrix} 1, \ldots, e^{j\frac{2\pi}{\lambda} r\left(p\, sin\boldsymbol{\phi}_{il}^r\, sin\boldsymbol{\theta}_{il}^r + q\, cos\boldsymbol{\theta}_{il}^r\right)}, \ldots, \\ e^{j\frac{2\pi}{\lambda} r\left(\left(\sqrt{N}-1\right) sin\boldsymbol{\phi}_{il}^r\, sin\boldsymbol{\theta}_{il}^r + \left(\sqrt{N}-1\right) cos\boldsymbol{\theta}_{il}^r\right)} \end{bmatrix}^T \tag{10}$$

$$\boldsymbol{T}_t \left(\boldsymbol{\phi}_{il}^t, \boldsymbol{\theta}_{il}^t\right)^H = \frac{1}{\sqrt{N}} \begin{bmatrix} 1, \ldots, e^{j\frac{2\pi}{\lambda} r\left(p\, sin\boldsymbol{\phi}_{il}^t sin\boldsymbol{\theta}_{il}^t + q\, cos\boldsymbol{\theta}_{il}^t\right)}, \ldots, \\ e^{j\frac{2\pi}{\lambda} r\left(\left(\sqrt{N}-1\right) sin\boldsymbol{\phi}_{il}^t\, sin\boldsymbol{\theta}_{il}^t + \left(\sqrt{N}-1\right) cos\boldsymbol{\theta}_{il}^t\right)} \end{bmatrix}^T \tag{11}$$

where r is the spacing between antennas and λ is the wavelength. For 2D-plane, the bounds of antenna indices p and q are $0 \leq p < \sqrt{N}$ and $0 \leq q < \sqrt{N}$, respectively. This model is applied in our simulations to make our hybrid precoder more applicable for general models.

C. PERFORMANCE METRICS

We consider that channel state information (CSI) is recognized for the BS and the MS. Practically, CSI is obtained effectively by channel estimation techniques. The spectral efficiency (SE) can be written as:

$$\mathrm{SE} = \log\det\left(I_{N_s} + \frac{\delta^2}{\sigma_n^2 N_s} \left(\mathbf{W}_{\mathrm{BB}}\mathbf{W}_{\mathrm{RF}}\right)^H \mathbf{P}\mathbf{F}_{\mathrm{RF}}\mathbf{F}_{\mathrm{BB}} \times \mathbf{F}_{\mathrm{RF}}^H\mathbf{F}_{\mathrm{BB}}^H\mathbf{P}^H \left(\mathbf{W}_{\mathrm{BB}}\mathbf{W}_{\mathrm{RF}}\right)\right) \tag{12}$$

where δ^2 is the phase noise variance. The $\mathbf{F}_{\boldsymbol{RF}}$ and $\mathbf{W}_{\boldsymbol{RF}}$ are implemented with phase shifters, which change the signal's phase. So their entries must achieve the constraints for nonzero elements, $\left|(\mathbf{F}_{\boldsymbol{RF}})_{i,j}\right| = \left|(\mathbf{W}_{\boldsymbol{RF}})_{i,j}\right| = 1$.

IV. DESIGN OF HYBRID PRECODER AND COMBINER

A. PROBLEM STATEMENT

It observed in [27] that the minimization of the Euclidean distance among the hybrid and the fully digital precoders is tractable and efficient alternative aim for spectral efficiency maximization of mm-wave systems. The precoders and combiners design can be divided into precoding sub-problems and combining sub-problems. The mathematical analysis is the same for the two sub-problems except that there is a power constraint in the optimization technique. Therefore, we analyze the precoder design in this article and the same analysis can be equally applied for the combiner design. The optimization problem for the design of hybrid precoder under phase noise in the proposed mmWave MIMO system is:

$$\begin{aligned} &\underset{\mathbf{F}_{\mathrm{RF}}, \mathbf{F}_{\mathrm{BB}}}{\text{minimize}} \quad \left\|\mathbf{F}_{\mathrm{opt}} - \delta^2\mathbf{F}_{\mathrm{RF}}\mathbf{F}_{\mathrm{BB}}\right\|_F^2 \\ &\text{Subject to} \begin{cases} \mathbf{F}_{\mathrm{RF}} \in \mathcal{A} \\ \left\|\delta^2\mathbf{F}_{\mathrm{RF}}\ \mathbf{F}_{\mathrm{BB}}\right\|_F^2 = N_S \end{cases} \end{aligned} \tag{13}$$

where $\mathbf{F}_{\mathrm{opt}}$ is the optimal digital precoder, $\mathbf{F}_{\mathrm{RF}}$ is the analog precoder and $\mathbf{F}_{\mathrm{BB}}$ is the digital precoder. The feasible set $\mathcal{A}$, is induced by the unit modulus constraints. It is observed in [26] that minimization of the optimization function results in maximizing the SE. We treat the problem in (13) as a matrix factorization problem and alternating minimization algorithm is used. Alternating minimization algorithm is applicable for many applications such as image reconstruction [53], deconvolution [54], matrix completion [55] and matrix factorization [56]. The optimization problem is a matrix factorization problem including two matrices $\mathbf{F}_{\mathrm{RF}}$ and $\mathbf{F}_{\mathrm{BB}}$. This technique can alternately solve for $\mathbf{F}_{\mathrm{RF}}$ and $\mathbf{F}_{\mathrm{BB}}$ while the other matrix is fixed.

B. DESIGN OF DIGITAL PRECODER $\mathbf{F}_{\mathrm{BB}}$

First, we solve the optimization problem for digital precoder, $\mathbf{F}_{\mathrm{BB}}$ while the matrix of analog precoder $\mathbf{F}_{\mathrm{RF}}$ is fixed. Thus, the problem in (13) becomes:

$$\underset{\mathbf{F}_{\mathrm{BB}}}{\text{minimize}} \quad \left\|\mathbf{F}_{\mathrm{opt}} - \delta^2\mathbf{F}_{\mathrm{RF}}\mathbf{F}_{\mathrm{BB}}\right\|_F \tag{14}$$

The ZF digital precoder is adopted with nearly optimal performance and $\mathbf{F}_{\mathrm{BB}}$ is given by:

$$\mathbf{G} = (\mathbf{H})^H \left(\mathbf{H}\,(\mathbf{H})^H\right)^{-1} \qquad \mathbf{F}_{\mathrm{BB}} = \beta\mathbf{G} \tag{15}$$

where $\beta = \sqrt{p} \big/ \left\|\mathbf{F}_{\mathrm{RF}}\mathbf{G}\right\|_F$ is the power normalized factor. The above solution in (15) has provided a near optimal solution to the digital precoder design.

C. DESIGN OF ANALOG PRECODER $\mathbf{F}_{\mathrm{RF}}$

The set $\mathcal{A}$ of RF precoder is expressed as $\left|(\mathbf{F}_{\mathrm{RF}})_{i,j}\right| = 1$, since every antenna is linked to all the RF chain. With the alternating minimization concept, we fix $\mathbf{F}_{\mathrm{BB}}$ and solve the optimization problem for $\mathbf{F}_{\mathrm{RF}}$ as follows:

$$\begin{aligned} &\underset{\mathbf{F}_{\mathrm{RF}}}{\text{minimize}} \quad \left\|\mathbf{F}_{\mathrm{opt}} - \delta^2\mathbf{F}_{\mathrm{RF}}\mathbf{F}_{\mathrm{BB}}\right\|_F^2 \\ &\text{Subject to} \quad \left|(\mathbf{F}_{\mathrm{RF}})_{i,j}\right| = 1, \quad \forall i, j. \end{aligned} \tag{16}$$

The unit modulus constraints are intrinsically non-convex. In this section, we apply manifold optimization technique to obtain a sub-optimal solution of the above problem (16). The background on manifold optimization is illustrated in [57]–[59]. Also, application of this algorithm can be found in [60].

1) DEFINITIONS AND TERMINOLOGIES FOR MANIFOLD OPTIMIZATION

Let $\mathcal{M}$ is the manifold space and $\mathrm{T}_x\mathcal{M}$ is the tangent space at a point x on the manifold $\mathcal{M}$ as shown in Fig. 2. Tangent space consists of tangent vectors ξ_x of the curves γ through the point x.

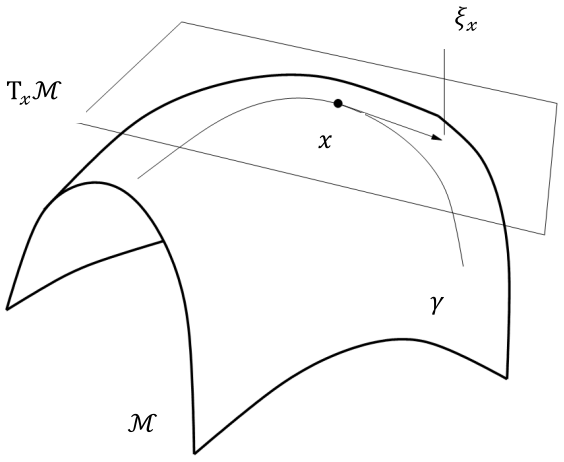

FIGURE 2. The tangent vector and space of manifold technique.

Let $\mathbb{C}$ denotes the complex plane with the Euclidean metric, which is given by:

$$\langle x_1 \, , \, x_2 \rangle = \Re \left\{ x_1^* \; x_2 \right\} \tag{17}$$

$$\mathcal{M}_{\mathrm{cc}} = \left\{ x \in \mathbb{C} : x^* x \right\} = 1 \tag{18}$$

At point $x \in \mathcal{M}_{\mathrm{cc}}$, the tangent space can be expressed as:

$$\mathrm{T}_x\mathcal{M}_{\mathrm{cc}} = \left\{ z \in \mathbb{C} : z^* x + x^* z = 2 \, \langle x \, , \, z \rangle = 0 \right\} \tag{19}$$

Let $\mathbf{x} = \mathrm{vec}\,(\mathbf{F}_{RF})$ is the vector of the analog precoder. It forms a complex circle manifold

$$\mathcal{M}_{cc}^{m} = \left\{ \mathbf{x} \in \mathbb{C}^m : |\mathbf{x}_1| = |\mathbf{x}_2| = \cdots = |\mathbf{x}_m| = 1 \right\} \tag{20}$$

where $m = N_t N_{RF}^t$. So, the problem search space is over a product m circles in the complex plane. Hence, the tangent space at a given point $\mathbf{x} \in \mathcal{M}_{cc}^{m}$ is:

$$\mathrm{T}_x\mathcal{M}_{cc}^{m} = \left\{ \mathbf{z} \in \mathbb{C}^m : \Re \left\{ \mathbf{z} \circ \mathbf{x}^* \right\} = 0_m \right\} \tag{21}$$

The gradient at point $\mathbf{x}$ is the tangent vector, $\mathrm{grad} f(\mathbf{x})$, determined by the Euclidean gradient orthogonal projection, $\nabla f(\mathbf{x})$ onto the space, $\mathrm{T}_x\mathcal{M}_{cc}^{m}$ [35]:

$$\mathrm{grad} f \; (\mathrm{x}) = \mathrm{Proj}_{\mathrm{x}} \nabla f \; (\mathbf{x}) \tag{22}$$

where the cost function gradient is

$$\nabla f \; (\mathrm{x}) = -2 \left(\mathbf{F}_{\mathrm{BB}}^* \otimes \mathbf{I}_{N_t} \right) \left[\mathrm{vec}(\mathbf{F}_{\mathrm{opt}}) - (\mathbf{F}_{\mathrm{BB}}^{\mathrm{T}} \otimes \mathbf{I}_{N_t}) \mathbf{x} \right] \tag{23}$$

The next step is *retraction*. It transforms a vector from the tangent space into the manifold zone.

It gives the destination on the manifold when moving through a tangent vector. The retraction can be described for a tangent vector $\alpha\mathbf{d}$ as follows:

$$\mathrm{Retr}_{\mathbf{x}} : \mathrm{T}_{\mathrm{x}}\mathcal{M}_{cc}^{m} \; \rightarrow \; \mathcal{M}_{cc}^{m} :$$

$$\alpha\mathbf{d} \longmapsto \mathrm{Retr}_{\mathrm{x}} \left(\alpha\mathbf{d} \right) = \mathrm{vec} \left[\frac{(\mathrm{x} + \alpha\mathbf{d})_i}{|(\mathrm{x} + \alpha\mathbf{d})_i|} \right] \tag{24}$$

To design the analog precoder, a line search based conjugate gradient algorithm is applied [36]. This algorithm uses Armijo backtracking search. Also, it uses the Polak-Ribiere variable to assure the objective function in each iteration to be non- increasing [37]. The Transport operation of a tangent vector $\mathbf{d}$ from $\mathbf{x}_k$ to $\mathbf{x}_{k+1}$ into two tangent spaces $\mathrm{T}_{\mathrm{x}_k}\mathcal{M}_{cc}^{m}$ and $\mathrm{T}_{\mathrm{x}_{k+1}}\mathcal{M}_{cc}^{m}$ is described as:

$$\mathrm{Transp}_{\mathrm{x}_k \rightarrow \mathrm{x}_{k+1}} : \mathrm{T}_{\mathrm{x}_k}\mathcal{M}_{cc}^{m} \; \rightarrow \; \mathrm{T}_{\mathrm{x}_{k+1}}\mathcal{M}_{cc}^{m} :$$

$$\mathbf{d} \longmapsto \mathbf{d} - \Re \left\{ \mathbf{d} \circ \mathrm{x}_{k+1}^* \right\} \circ \mathbf{x}_{k+1} \tag{25}$$

Algorithm 1 Alternating Minimization Algorithm

1: **Input:** $\mathbf{F}_{\mathrm{opt}}$, $\mathbf{F}_{\mathrm{BB}}^{(0)}$, $\mathbf{x}_0 \in \mathcal{M}_{cc}^{m}$
2: **Output:** $\mathbf{F}_{\mathrm{RF}}$ and $\mathbf{F}_{\mathrm{BB}}$
3: **Step 1: Analog Precoder Design** $\mathbf{F}_{\mathrm{RF}}$
4: $\mathbf{d}_0 = -\mathrm{grad} f \; (\mathbf{x}_0)$ and $k = 0$;
5: **for**
6: Put step size of Armijo backtracking α_k;
7: Apply the retraction process to obtain $\mathbf{x}_{k+1}$ as;

$$\mathbf{x}_{k+1} = \mathrm{Retr}_{\mathrm{x}_k}(\alpha_k \mathbf{d}_{\mathrm{k}});$$

8: Calculate the gradient

$$\mathbf{g}_{k+1} = \mathrm{grad} f \; (\mathbf{x}_{k+1}) \, ;$$

9: Determine the transport vectors $\mathbf{g}_k^+$ and $\mathbf{d}_k^+$ from x_k to x_{k+1};
10: Fix the parameter of Polak-Ribiere β_{k+1};
11: Calculate $\mathbf{d}_{k+1} = -\mathbf{g}_{k+1} + \beta_{k+1}\mathbf{d}_k^+$;
12: $k \leftarrow k + 1$;
13: **end**
14: **Step 2: Digital Precoder Design** $\mathbf{F}_{\mathrm{BB}}$
15: Initial $\mathbf{F}_{\mathrm{RF}}^{(0)}$ and let $k = 0$;
16: **for**
17: Determine $\mathbf{F}_{\mathrm{RF}}^{(\mathrm{k})}$ and $\mathbf{F}_{\mathrm{BB}}^{(\mathrm{k})} = \delta^{2^\dagger} \mathbf{F}_{\mathrm{RF}}^{(\mathrm{k})\dagger} \mathbf{F}_{\mathrm{opt}}$;
18: Solve $\mathbf{F}_{\mathrm{RF}}^{(\mathrm{k}+1)}$ using Algorithm 1 when $\mathbf{F}_{\mathrm{BB}}^{(\mathrm{k})}$ is calculated;
19: $k \leftarrow k + 1$;
20:**end**
21: Normalization, $\hat{\mathbf{F}}_{\mathrm{BB}} = \sqrt{N_{\mathrm{s}}} \mathbf{F}_{\mathrm{BB}} \Big/ \left\| \delta^2 \mathbf{F}_{\mathrm{RF}} \; \mathbf{F}_{\mathrm{BB}} \right\|_{\mathrm{F}}$

D. DESIGN OF HYBRID PRECODER

An alternating minimization algorithm is applied to design hybrid precoder. It is expressed in algorithm 1 by resolving

equations (14) and (16). The power constraint in (13) is achieved by normalizing the $\mathbf{F}_{\mathrm{BB}}$ at Step 21 of algorithm 1. The objective function in optimization problem (13) is minimized at Steps 17 and 18 in algorithm 1, each iteration will never increase it. The algorithm 1 may be utilized as a system performance benchmark in terms of SE.

V. THE PROPSED CHANNEL ESTIMATION TECHNIQUES

To minimize the effects of channel and phase noise issues, we suggest the MAP Estimator, LS Estimator, Bayesian Cramér-Rao Lower Bound Estimator and Kalman filter schemes.

A. MAP ESTIMATOR

This MAP estimator can estimates phase noise values $\boldsymbol{\Theta}$ by employing all received signals in the frame $\mathbf{y}$. This technique can maximize the posterior PDF log as follows:

$$\begin{aligned}
&\log p\left(\boldsymbol{\Theta} \mid \mathbf{y}\right) \\
&= \log\left\{\frac{p\left(\mathbf{y} \mid \boldsymbol{\Theta}\right) p\left(\boldsymbol{\Theta}\right)}{p\left(\mathbf{y}\right)}\right\} \\
&= \sum_{k=1}^{K}\left\{\log \frac{p\left(\boldsymbol{\Theta}\left(1\right)\right)}{\left(\pi\sigma_n^2\right)^{N_r}\left(2\pi\right)^{N/2}\left(\det\sum\right)^{1/2}}\right. \\
&\quad - \frac{\left[\boldsymbol{\Theta}\left(k\right)-\boldsymbol{\Theta}\left(k-1\right)\right]^H\sum^{-1}\left[\boldsymbol{\Theta}\left(k\right)-\boldsymbol{\Theta}\left(k-1\right)\right]}{2} \\
&\quad - \left[\mathbf{y}\left(k\right)-\boldsymbol{\Theta}^{[r]}\left(k\right)\mathbf{H}\boldsymbol{\Theta}^{[t]}\left(k\right)\bar{\mathbf{s}}\left(k\right)\right]^H\sum\nolimits_{\bar{n}(k)}^{-1} \\
&\quad \left.\times\left[\mathbf{y}\left(k\right)-\boldsymbol{\Theta}^{[r]}\left(k\right)\mathbf{H}\boldsymbol{\Theta}^{[t]}\left(k\right)\bar{\mathbf{s}}\left(k\right)\right]\right\} \\
&\quad - \log p\left(\mathbf{y}\right)
\end{aligned} \tag{26}$$

Since the two terms $\log\frac{p(\boldsymbol{\Theta}(1))}{(\pi\sigma_n^2)^{N_r}(2\pi)^{N/2}(\det\sum)^{1/2}}$ and $\log p\left(y\right)$ in equation (26) are independent of $\boldsymbol{\Theta}$, the phase noise estimation using MAP becomes:

$$\begin{aligned}
&\hat{\boldsymbol{\Theta}}^{[\mathrm{MAP}]} \\
&= \arg\min_{\boldsymbol{\Theta}}\sum_{k=1}^{K}\left\{\left[\mathbf{y}\left(k\right)-\boldsymbol{\Theta}^{[r]}\left(k\right)\mathbf{H}\boldsymbol{\Theta}^{[t]}\left(k\right)\bar{\mathbf{s}}\left(k\right)\right]^H\right. \\
&\quad \times\sum\nolimits_{\bar{n}(k)}^{-1}\left[y\left(k\right)-\boldsymbol{\Theta}^{[r]}\left(k\right)\mathbf{H}\boldsymbol{\Theta}^{[t]}\left(k\right)\bar{\mathbf{s}}\left(k\right)\right] \\
&\quad \left.+\frac{\left[\boldsymbol{\Theta}\left(k\right)-\boldsymbol{\Theta}\left(k-1\right)\right]^H\sum^{-1}\left[\boldsymbol{\Theta}\left(k\right)-\boldsymbol{\Theta}\left(k-1\right)\right]}{2}\right\}
\end{aligned} \tag{27}$$

where

- $\bar{\mathbf{s}}\left(k\right) \triangleq \mathbb{E}_{\mathcal{P}(k)}\left[\mathbf{S}\left(k\right)\right]$ represents the signal mean for the kth sampling instant;
- $\sum_{\bar{n}(k)} = \mathbb{E}\left[\bar{n}\left(k\right)\bar{n}^H\left(k\right)\right]$

$$\begin{aligned}
&= \boldsymbol{\Theta}^{[r]}\left(k\right)\mathbf{H}\boldsymbol{\Theta}^{[t]}\sum\nolimits_{\bar{s}(k)}\left(\boldsymbol{\Theta}^{[t]}\left(k\right)\right)^H \\
&\qquad \times H^H\left(\boldsymbol{\Theta}^{[r]}\left(k\right)\right)^H+\sigma_n^2\mathbf{I}_{N_rN_r}.
\end{aligned}$$

The computational complexity of the exhaustive search in (27) can be reduced into a series of 1-D searches by applying the alternating projection technique [64]. Thus, to obtain a proper initialization, $\hat{\boldsymbol{\Theta}}\left(k\right)$, is started by $0_{N\times 1}$, for $K = 1, 2, \ldots, K$, as the overall phase noise matrix and channel gains processes are evaluated at the beginning of each frame.

B. LS ESTIMATOR

This sub-section derives an LS estimator of phase noise and channels parameters. The main function is to reduce the square distance between the transmitted and received signals. The received signal likelihood function, $\boldsymbol{y}$ in terms of the phase noise $\boldsymbol{\Theta}$ and channel magnitudes $\mathbf{H}$ is described as:

$$\begin{aligned}
p\left(\mathbf{y} \mid \mathbf{H}, \boldsymbol{\Theta}\left(\mathbf{n}\right)\right) &= \frac{1}{\left(\pi\right)^{L_tN_r}\det\left(\mathbf{C}_y\right)} \\
&\quad \times\exp\left\{-\left(\mathbf{y}-\boldsymbol{\mu}_{bmy}\right)^H\mathbf{C}_{\mathrm{y}}^{-1}\left(\mathbf{y}-\boldsymbol{\mu}_{\boldsymbol{y}}\right)\right\}
\end{aligned} \tag{28}$$

where $\boldsymbol{\mu}_{\mathbf{y}}$ is the mean and $\mathbf{C}_y$ is the covariance matrix. The joint LS estimates of phase noise $\boldsymbol{\Theta}\left(\mathbf{n}\right)$ and channel gains $\mathbf{H}$ is:

$$\hat{\mathbf{H}}, \hat{\boldsymbol{\Theta}}\left(\mathbf{n}\right) = \arg\min_{\mathbf{H},\boldsymbol{\Theta}}\left(\mathbf{y}-\mu_y\right)^H\left(\mathbf{y}-\mu_y\right) \tag{29}$$

Then, the cost function became:

$$\hat{\mathbf{H}}, \hat{\boldsymbol{\Theta}}\left(\mathbf{n}\right) = \arg\min_{\mathbf{H},\boldsymbol{\Theta}}\left(\mathbf{Y}-\mathbf{P}\left(n\right)\mathbf{S}\right)^H\left(\mathbf{Y}-\mathbf{P}\left(n\right)\mathbf{S}\right) \tag{30}$$

where $\mathbf{P}\left(n\right)$ **is** defined in (6) and $\mathbf{S} \triangleq \left[\mathbf{s}_1, \ldots, \mathbf{s}_{N_t}\right]^T$ is an $N_t \times L_t$ matrix. The LS estimate of $\mathbf{P}\left(n\right)$, $\hat{\mathbf{P}}\left(n\right)$ is:

$$\hat{\mathbf{P}}\left(n\right) = \mathbf{Y}\mathbf{S}^H\left(\mathbf{S}\mathbf{S}^H\right)^{-1} = \frac{\mathbf{Y}\mathbf{S}^H}{L_t} \tag{31}$$

Using (31), estimates of the phase noise and channel magnitude matrices, respectively are calculated by:

$$\hat{\boldsymbol{\Theta}}\left(\mathbf{n}\right) = \angle\left\{\frac{\mathbf{Y}\mathbf{S}^H}{L_t}\right\} \tag{32}$$

$$\hat{\mathbf{H}} = \frac{\left|\mathbf{Y}\mathbf{S}^H\right|}{L_t} \tag{33}$$

where $\angle\left\{\cdot\right\}$ returns the phase of variable and $|\cdot|$ is the absolute value operator.

C. BAYESIAN CRAMER-RAO LOWER BOUND

To recover the transmitted signal at time instant n, $\mathbf{s}\left(n\right)$, the receiver with BCRLBs can estimates the phase noise parameters, $\Theta_k\left(n\right)$ for $k = 1, \ldots, N_r$. This subsection derives the BCRLBs for phase noise estimation. It is calculated by taking the inverse of Fisher's information matrix [65]–[67]:

$$\mathbf{BCRLB}\left(\boldsymbol{\Theta}\right) = \mathrm{diag}\left(\mathbf{FIM}^{-1}\right) \tag{34}$$

where **FIM** is the $N_t \times N_r$ Fisher's information matrix (FIM) [67]. We first explain the *Proposition* 1 to calculate the FIM.

Proposition 1: The $N_t \times N_r$ FIM for the phase estimation is:

$$\mathbf{FIM}_{k,\bar{k}} = \left[\frac{\partial \mu(\mathbf{\Theta})}{\partial \mathbf{\Theta}_k}\right]^T \mathbf{C}_{\mathbf{y}}^{-1}(\mathbf{\Theta}) \left[\frac{\partial \mu(\mathbf{\Theta})}{\partial \mathbf{\Theta}_{\bar{k}}}\right] + \frac{1}{2}\mathrm{Tr}\left[\mathbf{C}_{\mathbf{y}}^{-1}(\mathbf{\Theta}) \frac{\partial \mathbf{C}_{\mathbf{y}}(\mathbf{\Theta})}{\partial \mathbf{\Theta}_k(n)} \mathbf{C}_{\mathbf{y}}^{-1}(\mathbf{\Theta}) \frac{\partial \mathbf{C}_{\mathbf{y}}(\mathbf{\Theta})}{\partial \mathbf{\Theta}_{\bar{k}}(n)}\right]; \quad k, \bar{k} = 1, \ldots, N_r \tag{35}$$

where

- $\frac{\partial \mu(\mathbf{\Theta})}{\partial \mathbf{\Theta}_k} \triangleq \left[\mathbf{0}^T_{(k-1)L_t \times N_t}, (\Xi_k \mathbf{s})^T, \mathbf{0}^T_{(N_r-k)L_t \times N_t}\right]^T$ is an $N_r L_t \times N_t$ matrix, which denotes to derivative of the received signal mean with respect to phase noise;
- The mean is given by, $\mu(\mathbf{\Theta}) = \sum_{l=1}^{N_t} \mathrm{A}_{k,l} e^{j\mathrm{B}_{k,l}} \mathbf{s}_l$;
- $\mathbf{s} \triangleq \left[s^T(1), \ldots, s^T(N_t)\right]^T$ is an $N_t \times L_t$ matrix;
- $\frac{\partial \mathbf{C}_{\mathbf{y}}(\mathbf{\Theta})}{\partial \mathbf{\Theta}_k(n)}$ denotes to derivative of the covariance matrix with respect to phase noise;
- $\mathbf{C}_{\mathbf{y}}^{-1}$ is the inverse of received signal covariance matrix.
- $\mathbf{C}_{\mathbf{y}}$ is the $N_r L_t \times N_r L_t$ covariance matrix of received signal, $\mathbf{y}$.

After taking the expectation and making some mathematical processing, the covariance matrix becomes:

$$\mathbf{C}_{y_{k,\bar{k}}} = \begin{cases} \sum_{l=1}^{N_t} h_{k,l}^2 \mathbf{s}_l \mathbf{s}_l^H \left(\sigma_{\vartheta_l}^2 \mathbf{T} + \sigma_{\vartheta_k}^2 \mathbf{T}\right) \\ + \sum_{l=1}^{N_t} \sum_{\bar{l}=1, \bar{l} \neq l}^{N_t} \left|h_{k,l}\right| \left|h_{\bar{k},\bar{l}}\right| \times e^{j\left[\Theta_{k,l}(n) - \Theta_{\bar{k},\bar{l}}(n)\right]} \\ \times \mathbf{s}_l \mathbf{s}_{\bar{l}}^H \left(\sigma_{\vartheta_k}^2 \mathbf{T}\right) + \sigma_w^2 \mathbf{I}_{L_t \times L_t}, \quad k = \bar{k} \\ \sum_{l=1}^{N_t} \left|h_{k,l}\right| \left|h_{\bar{k},l}\right| \times e^{j\left[\Theta_{k,l}(n) - \Theta_{\bar{k},l}(n)\right]} \mathbf{s}_l \mathbf{s}_{\bar{l}}^H \\ \odot \left(\sigma_{\vartheta_l}^2 \mathbf{T}\right), \quad k \neq \bar{k} \end{cases} \tag{36}$$

where $\mathbf{T}$ is an $L_t \times L_t$ matrix given by:

$$\mathbf{T} = \begin{bmatrix} L_t - 1 & L_t - 2 & \cdots & 0 \\ L_t - 2 & L_t - 2 & \cdots & 0 \\ \vdots & \vdots & \ddots & \vdots \\ 0 & 0 & \cdots & 0 \end{bmatrix} \tag{37}$$

and

$$T_{k,l} \triangleq \left[\sum_{m=n-L_t+2}^{n} \left[\vartheta_l^t(m) + \vartheta_k^r(m)\right], \sum_{m=n-L_t+3}^{n} \left[\vartheta_l^t(m) + \vartheta_k^r(m)\right], \ldots, 0\right]^T \tag{38}$$

The partitioned matrix inverse of **FIM** in (34) is used to obtain the CRLB closed-form expression for specific N_r and N_t values. After taking the matrix inversion of **FIM**,its diagonal elements gives the BCRLB for the estimation of phase noise.

VI. TRACKING PHASE NOISE

To track the phase noise in mmWave MIMO system, we propose Kalman filter scheme. First, the state and observation are calculated for the KF. The overall phase noise is:

$$\mathbf{\Theta}_{k,l}(n) = \mathbf{\Theta}_{k,l}(n-1) + \Delta_{k,l}(n) \tag{39}$$

where $\Delta_{k,l}(n) = \Delta_l^{[t]}(n) + \Delta_l^{[r]}(n)$ is total phase noise rate. The unknown state vector is:

$$\mathbf{\Theta}(n) = \left[\mathbf{\Theta}_1^T(n), \ldots, \mathbf{\Theta}_{N_r}^T(n)\right]^T = \mathbf{\Theta}(n-1) + \boldsymbol{\vartheta}(n) \tag{40}$$

where $\boldsymbol{\vartheta}(n) = \left[\vartheta_{1,1}(n), \ldots, \vartheta_{N_r,N_t}(n)\right]^T$ is the state noise vector, which has zero mean and variance $\mathbf{Q}$. It is calculated as follows:

$$\mathbf{Q} = \mathbb{E}\left\{\boldsymbol{\vartheta}(n) \boldsymbol{\vartheta}(n)^T\right\} \tag{41}$$

In matrix form, Eq. (41) can be expressed as:

$$\mathbf{Q} = \begin{bmatrix} \mathbf{Q}_{1,1} & \cdots & \mathbf{Q}_{1,N_r} \\ \vdots & \ddots & \vdots \\ \mathbf{Q}_{N_r,1} & \cdots & \mathbf{Q}_{N_r,N_r} \end{bmatrix} \tag{42}$$

where

$$\mathbf{Q}_{k,\bar{k}} = \begin{cases} \sigma_{\vartheta_k}^2 \cdot \mathbf{I}_{N_t \times N_t} + \mathrm{diag}\left(\sigma_{\vartheta_1}^2, \cdots, \sigma_{\vartheta_{N_t}}^2\right), & k = \bar{k} \\ \mathrm{diag}\left(\sigma_{\vartheta_1}^2, \cdots, \sigma_{\vartheta_{N_t}}^2\right), & k \neq \bar{k} \end{cases} \tag{43}$$

From equation (5), the received signal for the Kalman filter is:

$$\mathbf{y}(n) = \mathbf{x}(n) + \mathbf{w}(n) \tag{44}$$

where

- $\mathbf{x}(n) = \mathbf{W}_{\mathrm{BB}}^H \mathbf{W}_{\mathrm{RF}}^H \left(\mathbf{A} \odot \mathbf{e}^{j\mathbf{B}(n)}\right) \mathbf{F}_{\mathrm{RF}} \mathbf{F}_{\mathrm{BB}} \mathbf{s}(n)$
- $\mathbf{w}(n) = \mathbf{W}_{\mathrm{BB}}^H \mathbf{W}_{\mathrm{RF}}^H \mathbf{n}(n)$

The received signal in the above equation can be seen as a non-linear function of the unknown state vector $\mathbf{\Theta}$. So, we apply KF scheme in order to linearize it [68]. So, the Jacobian matrix is determined through calculating the 1st order partial derivative of $\mathbf{x}(n)$ with respect to the $\mathbf{\Theta}(n)$ as:

$$\boldsymbol{J} = \frac{\partial \mathbf{x}(\mathrm{n})}{\partial \mathbf{\Theta}^T(\mathrm{n})} = \begin{bmatrix} \frac{\partial x_1(n)}{\partial \beta_1^T(n)} & \mathbf{0}_{1 \times N_t} & \cdots & \mathbf{0}_{1 \times N_t} \\ \mathbf{0}_{1 \times N_t} & \frac{\partial x_2(n)}{\partial \beta_2^T(n)} & \cdots & \mathbf{0}_{1 \times N_t} \\ \vdots & \vdots & \ddots & \vdots \\ \mathbf{0}_{1 \times N_t} & \mathbf{0}_{1 \times N_t} & \cdots & \frac{\partial x_{N_r}(n)}{\partial \beta_{N_r}^T(n)} \end{bmatrix} \tag{45}$$

Let $\mathbf{M}(n \mid n-1)$ and $\mathbf{K}(n)$ are the prediction error covariance matrix and the Kalman gain. After initialization step, the KF scheme is processed as follows. The predicted state vector of phase noise is:

$$\tilde{\mathbf{\Theta}}(n \mid n-1) = \tilde{\mathbf{\Theta}}(n-1 \mid n-1) \tag{46}$$

and the prediction error covariance matrix is:

$$\mathbf{M}(n \mid n-1) = \mathbf{M}(n-1 \mid n-1) + \mathbf{Q} \tag{47}$$

Then, the Kalman gain can be calculated as:

$$\mathbf{K}(n) = \mathbf{M}(n \mid n-1)\, \boldsymbol{J}^{H}(\boldsymbol{\Theta}(n \mid n-1)) \times \left(\boldsymbol{J}(\boldsymbol{\Theta}(n \mid n-1))\, \mathbf{M}(n \mid n-1)\, \boldsymbol{J}^{H}(\boldsymbol{\Theta}(n \mid n-1)) + \sigma^{2}\mathbf{I}\right)^{-1} \quad (48)$$

After that, the proposed Kalman filter refines the scores by the backward-recursive equations, for phase noise and error covariance matrix:

$$\tilde{\boldsymbol{\Theta}}(n \mid n) = \tilde{\boldsymbol{\Theta}}(n \mid n-1) + \Re\{\mathbf{K}(n) \times [\mathbf{y}(n-1) -]\left(\hat{\mathbf{A}} \odot \mathbf{e}^{j\hat{\mathbf{B}}(\mathrm{n})}\right)\mathbf{s}(n-1)\} \quad (49)$$

$$\mathbf{M}(n \mid n) = \Re\{\mathbf{M}(n \mid n-1) - \mathbf{K}(n)\,(\boldsymbol{\Theta}(n \mid n-1)) \times \mathbf{M}(n \mid n-1)\} \quad (50)$$

where

- $\boldsymbol{J}(\boldsymbol{\Theta}(n \mid n-1)) = \boldsymbol{J}(\boldsymbol{\Theta}(n))|_{\boldsymbol{\Theta}(n)=\hat{\boldsymbol{\Theta}}(n|n-1)}$ is the Jacobian matrix and is given in equation (45).
- $\hat{\boldsymbol{\Theta}}(n \mid n-1)$ is the predicted state vector for the nth symbol
- $\hat{\mathbf{B}}(\mathrm{n}) = \mathbf{B}(\mathrm{n})|_{\boldsymbol{\Theta}(n)=\hat{\boldsymbol{\Theta}}(n|n-1)}$ is the estimated phase shift.

VII. MODEL OF POWER CONSUMPTION

Power consumption model is important for describing different components and devices in mmWave MIMO system and their power consumption. The total power consumptions of each component in mmWave MIMO system, P_T is:

$$P_T = P_{PA} + N_r P_{LNA} + L_r\,(P_{\text{RF chain}} + P_{ADC}) + P_{BB} \quad (51)$$

where

- P_{PA} is the he power dissipated in the passed array and is given by:

$$P_{PA} = N_r \times L_r \times P_{\text{RF shifter}} \quad (52)$$

  where $P_{\text{RF shifter}}$ is the power consumption shifters. Its value is based on the kind and resolution of the quantized phases. In [73], a power consumption shifter $P_{\text{RF shifter}}$ of 20 mW is suggested for each phase shifter.
- $P_{\text{RF chain}}$ is the power consumed by the RF chain, which includes a local oscillator, a mixer, a base band amplifier and a low pass filter. The authors in [74] considered values of 14mW and 5mW for low pass filter and base band amplifier, respectively. An oscillator phase noise is inversely proportional to the power consumption. In [75], [76], the oscillator power consumption is 60 mW for each element in the voltage controlled oscillator. Signal power from oscillator is used to drive the mixer, which consumes 10 mW. Then, the total power consumption for the oscillator is 70 mW. In [77], the power consumption of voltage controlled oscillator is 122 mW. It is measured under phase noise at the oscillation frequency varies from 26.46 to 28.90 GHz. It is calculated as follows:

$$P_{\text{RF chain}} = P_{LO} + P_{mixer} + P_{BB\ amp} + P_{LPF} \quad (53)$$

TABLE 2. Values of ADC power consumption.

Ref.	Sampling rate [Gs/s]	Band width [GHz]	Eff. number of bits	Power consumption [mW]
[69]	1.25	> 0.6	6.7	207
[70]	1.8	> 0.8	5.1	30
[71]	2.2	> 1	7	27.4
[72]	2.5	> 1	4.9	98

- P_{ADC} is the power consumed by single analog to digital converter. Power consumption of ADC versus sampling frequency, effective bits number, and bandwidth for various studies are listed in TABLE 1. We assume a value of 200 mW.
- P_{LNA} is the power consumed by a single low noise amplifier. Studies for the low power LNAs at 60 GHz band in CMOS technology and mmWave MIMO system illustrate that power consumption is in the range of 10 to 86 mW. In our work, we consider 20 mW for the proposed system.
- P_{BB} is the power consumption of baseband precoder/combiner. The baseband processor of precoder/combiner consumes 200 mW.

Finally, we compare the power consumption of an ideal system [14] and proposed scheme to show the impact of phase noise problem as in Fig. 3. In Fig. 3, the power consumption for ideal system [14] and proposed system is compared. When the number of antennas increases, the power consumption is decreased.

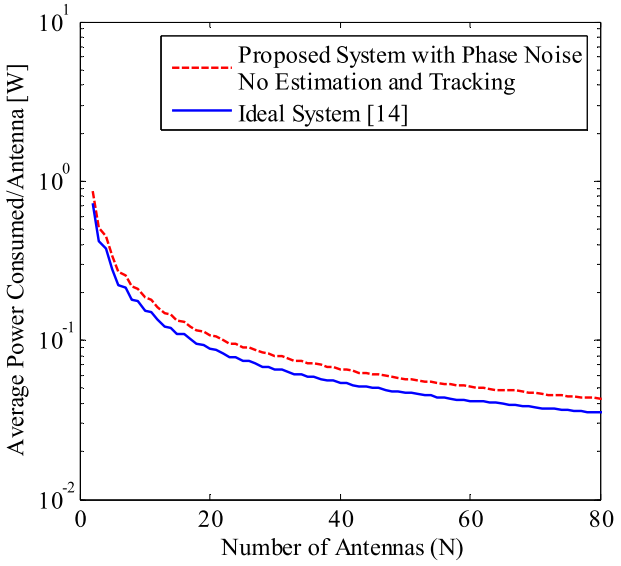

FIGURE 3. Average power consumption vs. number of antennas (N_t) of ideal system [14] and non-ideal proposed system with phase noise, $\delta = 10^{-3}\text{rad}^2$.

VIII. RESULTS

The SE performance of our proposed mmWave MIMO system is evaluated numerically and analytically. All resulted

figures are extracted from analytical equations that match well with the marker symbols extracted from the simulation. The information are forwarded from the transmitter with $N_t = 64$ to the receiver with $N_r = 16$ antennas. A uniform square planar array is deployed at both transmitter and receiver. The parameters of the channel are $N_{\text{clusters}} = 5$, $N_{\text{rays}} = 10$ and the average power is $\sigma^2_{\alpha,i} = 1$. We assume the distribution of the azimuth and elevation angles is Laplacian with mean angles and angular spread of 10 degrees. The elements of antenna in the array of uniform square planar are disconnected by a half wavelength distance. In [23], the authors studied the devices for communication system under phase noise and make measurements at 2.8 GHz with $T_s = 10^{-6}$sec and variance of phase noise equals $\delta = 10^{-4}$ rad^2. Consider that $\delta = 10^{-4}$rad^2 represents the lowest impact of phase noise problem and $\delta = 10^{-2}$ rad^2 is the greatest effect of phase noise problem. To estimate the phases and channel gains at time n, we apply the proposed LS algorithm at the beginning of data. Then, we initialize the state model of the Kalman filter algorithm using these estimates and calculate the next estimates of phase noise at time $n+1$ and so on. We examine the impact of the suggested mmWave MIMO system with MAP estimator, LS estimator, BCRLBs and Kalman filter algorithms in terms of SE performance.

A. IMPACT OF CHANGING RF CHAINS

Firstly, we show the spectral efficiency achieved by MAP estimator, LS estimator, BCRLBs and Kalman filter algorithms when the number of RF chains is $L_t = L_r = 3$ and $\delta = 10^{-2}$ rad^2 as shown in Fig. 4.

The authors in [14] studied the ideal scenario of mmWave system without hardware problems. The ideal mmWave is a reference to evaluate the proposed scheme performance. The proposed system with LS achieves lower spectral efficiency than the other algorithms. On the contrary, BCRLBs algorithm can give near-optimal performance over the whole SNR range and close to the ideal case [14]. At low number of RF chains, there is an enhancement in the SE performance with using BCRLBs algorithm. It approaches to the ideal mmWave system [14]. The proposed MAP estimator can provide substantial performance gains over LS and Kalman filter, especially at high SNRs as in Fig. 4. When the RF chains number increased (i.e., $L_t = L_r = 10$) with the same value of phase noise $\delta = 10^{-2}$ rad^2, there exists a gain in the system performance as illustrated in Fig. 5. The LS estimator decreases the effect of phase noise, but its performance is quite far from the ideal system [14]. At low SNRs, the MAP estimator gives the same performance of the Kalman filter. BCRLBs algorithm can give the better performance.

B. IMPACT OF CHANGING DIFFERENT-PATH CHANNELS

Fig. 6 and Fig. 7 show different path channel scenarios for three and ten paths, respectively. For the three paths scenario, the proposed system with estimation methods shows the same performance. MAP, LS, BCRLBs and Kalman filter

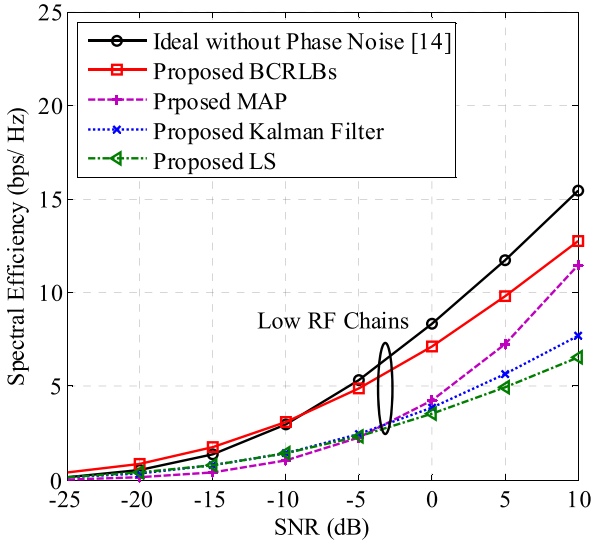

FIGURE 4. Spectral efficiency of different estimation algorithms at $\delta = 10^{-2}$rad^2 and RF chains number $L_t = L_r = 3$.

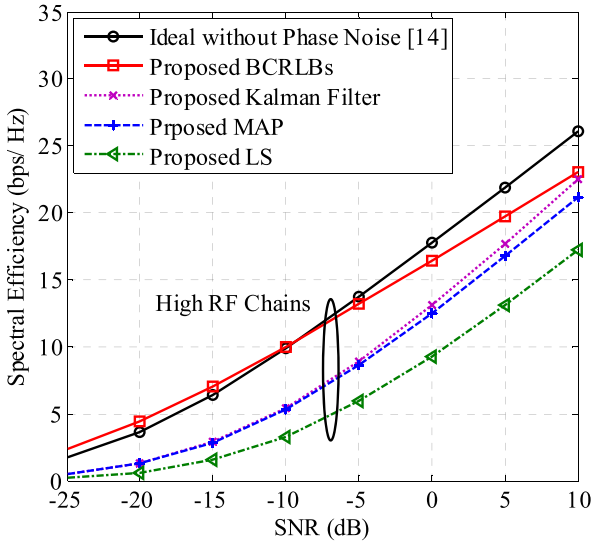

FIGURE 5. Spectral efficiency of different estimation algorithms at $\delta = 10^{-2}$rad^2 and RF chains number $L_t = L_r = 10$.

algorithms can improve the system performance and closes to the ideal system performance with the range of 0dB to 5dB as in Fig. 6. These algorithms can decrease the impact of phase noise. At SNR = 5dB, the SE is 8.5 bps/Hz for LS estimator, which is close to SE = 9 bps/Hz for the ideal system as in Fig. 6. In Fig. 7, there exists a large performance gap among the estimation algorithms when the RF chains number is increased to 10 as shown in Fig. 7. This scenario is a real study case, for recent estimation campaigns in mmWave bands, which demonstrate that channels in a city environment may be evaluated using a pre-estimated paths cluster number [75], [76]. The proposed MAP, BCRLBs and Kalman filter outperform LS scheme. The performance of LS algorithm becomes worse in multipath environment, because of lacking in exploiting multipath channel gains. The performance of the mmWave system worsens when the system is operated under

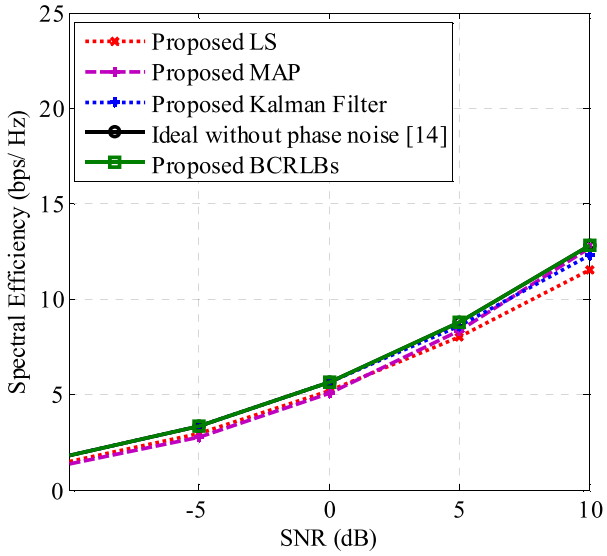

FIGURE 6. SE vs. SNR of ideal system [14] and suggested scheme with phase noise problem at $N_t = 64$, $N_r = 16$, channel paths = 3 and $N_s = 4$ data streams.

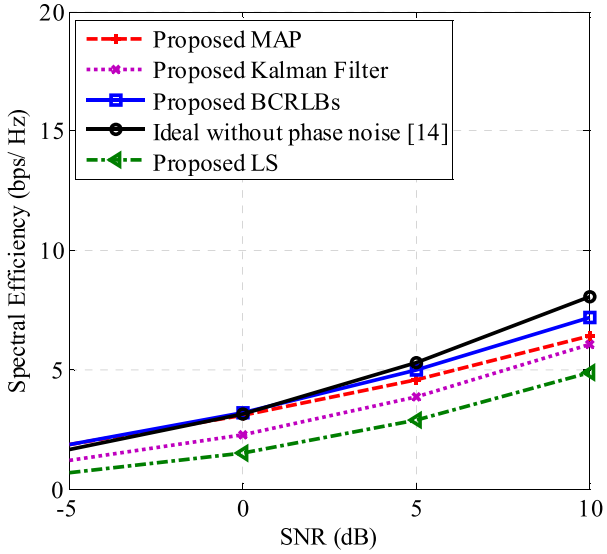

FIGURE 7. SE vs. SNR of ideal system [14] and suggested scheme with phase noise problem at $N_t = 64$, $N_r = 16$, channel paths = 10 and $N_s = 4$ data streams.

phase noise problem and higher number of channel paths. The SE performance is far from the ideal system.

C. IMPACT OF CHANGING PHASE NOISE

This subsection analyzes the effect of different variances of phase noise for mmWave system. Fig. 8 shows the SE achieved with the proposed MAP estimator, LS estimator, BCRLBs and Kalman filter together with the SE without channel estimation [14]. At low phase noise, BCRLBs algorithm always has the highest SE under different system parameters. With SNR = 0 dB, the ideal system SE is 23 bps/Hz, which is higher than 21, 19, 17 and 14 bps/Hz for the proposed system with BCRLBs, Kalman filter, MAP and LS, respectively, as illustrated in Fig. 8.

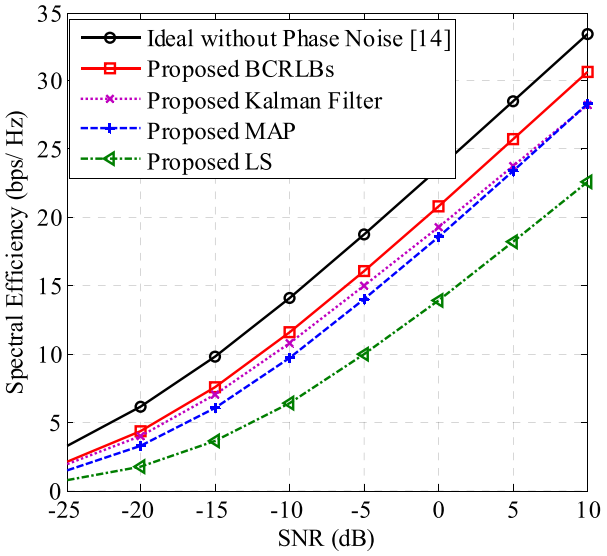

FIGURE 8. SE vs. SNR of ideal system [14] and suggested scheme in low phase noise, $\delta = 10^{-4}$ rad^2.

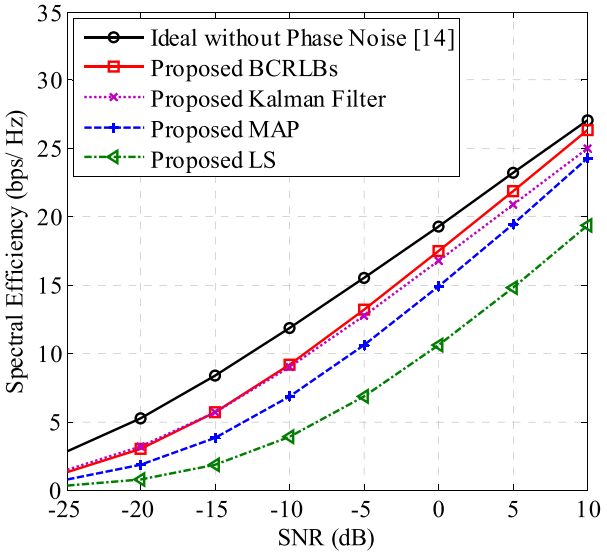

FIGURE 9. SE vs. SNR of ideal system [14] and suggested scheme in low phase noise, $\delta = 10^{-3}$rad^2.

When the phase noise is increased, $\delta = 10^{-3}$ rad^2, SE performance is much less as shown in Fig. 9. With SNR = 0 dB, SE for ideal system is 19 bps/Hz, which is higher than 17, 16.5, 15 and 10 bps/Hz for the proposed system with BCRLBs, Kalman filter, MAP and LS, respectively, as shown in Fig. 9. There is a loss in the performance between Figs. 8 and 9. We can conclude that SE performance of proposed system varies with changing the phase noise. It is obvious that performance of mmWave MIMO system is extremely affected. As a result, we must design devices at the least defect of phase noise to obtain good SE performance.

We also compare the proposed system with [46], which studies the system under non-ideal hardware as in Fig. 10. The phase noise problem gives very low SE compared to the amplified thermal noise, and the residual additive transceiver

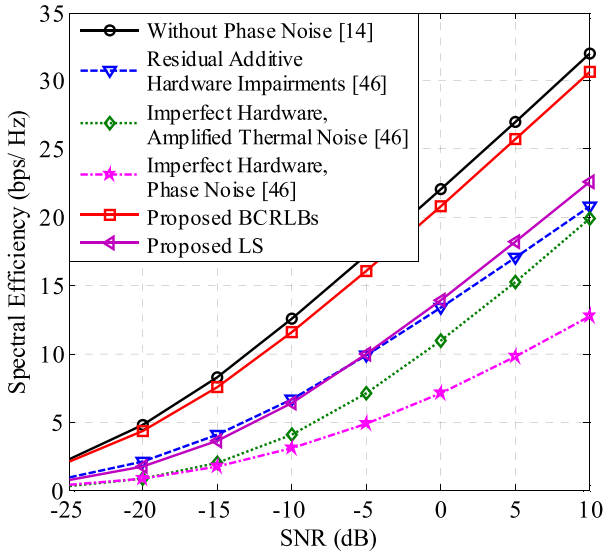

FIGURE 10. SE vs. SNR of ideal system [14], imperfect hardware [46] and suggested scheme (Case: phase noise, $\delta = 10^{-2}\text{rad}^2$, amplified thermal noise, $\xi = 0.5\sigma^2$, residual additive impairments, $\kappa^2 = 0.1$).

impairments in [46]. The problem of residual additive impairments, which arises from the antenna coupling, the quantization noise in the ADCs and the DC offset has lower impact on the SE performance compared to amplified thermal noise. The ideal hardware scenario in [14] is taking a benchmark to measure SE performance. The proposed system with LS and BCRLBs solution can enhance the Wave system under hardware problems. The performance of mmWave system is affected by phase noise. So, the hardware comments of mmWave system should be designed with good quality.

IX. CONCLUSION

In this article, mmWave MIMO system under hardware imperfection has been proposed. A realistic power consumption model has been assumed. An optimization problem is formulated to design hybrid precoding using an alternating minimization algorithm. A BCRLBs, Kalman filter, LS and MAP algorithms have been proposed for estimating and tracking phase noise and channel gains parameters. Comparison between proposed system and non-ideal hardware mmWave system has been illustrated under different scenarios. Results confirmed that mmWave MIMO system with proposed algorithms can mitigate the problems of non-ideal hardware.

REFERENCES

[1] D. Ciuonzo, P. S. Rossi, and S. Dey, "Massive MIMO channel-aware decision fusion," *IEEE Trans. Signal Process.*, vol. 63, no. 3, pp. 604–619, Feb. 2015.

[2] F. Jiang, J. Chen, A. L. Swindlehurst, and J. A. Lopez-Salcedo, "Massive MIMO for wireless sensing with a coherent multiple access channel," *IEEE Trans. Signal Process.*, vol. 63, no. 12, pp. 3005–3017, Jun. 2015.

[3] A. Shirazinia, S. Dey, D. Ciuonzo, and P. S. Rossi, "Massive MIMO for decentralized estimation of a correlated source," *IEEE Trans. Signal Process.*, vol. 64, no. 10, pp. 2499–2512, May 2016.

[4] T. S. Rappaport, S. Sun, R. Mayzus, H. Zhao, Y. Azar, K. Wang, G. N. Wong, J. K. Schulz, M. Samimi, and F. Gutierrez, "Millimeter wave mobile communications for 5G cellular: It will work!" *IEEE Access*, vol. 1, pp. 335–349, 2013.

[5] S. Mumtaz, J. Rodriguez, and L. Dai, *mmWave Massive MIMO: A Paradigm for 5G*. New York, NY, USA: Academic, 2016.

[6] J. G. Andrews, S. Buzzi, W. Choi, S. V. Hanly, A. Lozano, A. C. K. Soong, and J. C. Zhang, "What will 5G be?" *IEEE J. Sel. Areas Commun.*, vol. 32, no. 6, pp. 1065–1082, Jun. 2014.

[7] G. R. MacCartney, S. Deng, S. Sun, and T. S. Rappaport, "Millimeter-wave human blockage at 73 GHz with a simple double knife-edge diffraction model and extension for directional antennas," in *Proc. IEEE 84th Veh. Technol. Conf. (VTC-Fall)*, Sep. 2016, pp. 1–6.

[8] M. Rebato, M. Mezzavilla, S. Rangan, F. Boccardi, and M. Zorzi, "Understanding noise and interference regimes in 5G millimeter-wave cellular networks," in *Proc. Eur. Wireless Conf.*, May 2016, pp. 1–5.

[9] H. Shokri-Ghadikolaei and C. Fischione, "Millimeter wave ad hoc networks: Noise-limited or interference-limited?" in *Proc. IEEE Globecom Workshops (GC Wkshps)*, Dec. 2015, pp. 1–7.

[10] Z. Mokhtari, M. Sabbaghian, and R. Dinis, "A survey on massive MIMO systems in presence of channel and hardware impairments," *Sensors*, vol. 19, no. 1, p. 164, Jan. 2019.

[11] T. Xie, L. Dai, D. W. K. Ng, and C.-B. Chae, "On the power leakage problem in millimeter-wave massive MIMO with lens antenna arrays," *IEEE Trans. Signal Process.*, vol. 67, no. 18, pp. 4730–4744, Sep. 2019.

[12] A. Thornburg, T. Bai, and R. W. Heath, Jr., "Interference statistics in a random mmWave ad hoc network," in *Proc. IEEE Int. Conf. Acoust., Speech Signal Process. (ICASSP)*, Apr. 2015, pp. 2904–2908.

[13] Y. Han and J. Lee, "Two-stage compressed sensing for millimeter wave channel estimation," in *Proc. IEEE Int. Symp. Inf. Theory (ISIT)*, Barcelona, Spain, Jul. 2016, pp. 860–864.

[14] A. Alkhateeb, O. El Ayach, G. Leus, and R. W. Heath, Jr., "Channel estimation and hybrid precoding for millimeter wave cellular systems," *IEEE J. Sel. Topics Signal Process.*, vol. 8, no. 5, pp. 831–846, Oct. 2014.

[15] D. Petrovic, W. Rave, and G. Fettweis, "Effects of phase noise on OFDM systems with and without PLL: Characterization and compensation," *IEEE Trans. Commun.*, vol. 55, no. 8, pp. 1607–1616, Aug. 2007.

[16] A. Garcia-Rodriguez, V. Venkateswaran, P. Rulikowski, and C. Masouros, "Hybrid analog–digital precoding revisited under realistic RF modeling," *IEEE Wireless Commun. Lett.*, vol. 5, no. 5, pp. 528–531, Oct. 2016.

[17] E. Costa and S. Pupolin, "M-QAM-OFDM system performance in the presence of a nonlinear amplifier and phase noise," *IEEE Trans. Commun.*, vol. 50, no. 3, pp. 462–472, Mar. 2002.

[18] T. Schenk, *RF Imperfections in High-Rate Wireless Systems: Impact and Digital Compensation*. Berlin, Germany: Springer, 2008.

[19] C. Studer, M. Wenk, and A. Burg, "MIMO transmission with residual transmit-RF impairments," in *Proc. Int. ITG Workshop Smart Antennas (WSA)*, Feb. 2010, pp. 189–196.

[20] E. Bjornson, P. Zetterberg, M. Bengtsson, and B. Ottersten, "Capacity limits and multiplexing gains of MIMO channels with transceiver impairments," *IEEE Commun. Lett.*, vol. 17, no. 1, pp. 91–94, Jan. 2013.

[21] E. Bjornson and E. Jorswieck, "Optimal resource allocation in coordinated multi-cell systems," *Found. Trends Commun. Inf. Theory*, vol. 9, nos. 2–3, pp. 113–381, 2013.

[22] U. Gustavsson, C. Sanchez-Perez, T. Eriksson, F. Athley, G. Durisi, P. Landin, K. Hausmair, C. Fager, and L. Svensson, "On the impact of hardware impairments on massive MIMO," in *Proc. IEEE Globecom Workshops (GC Wkshps)*, Dec. 2014, pp. 294–300.

[23] A. K. Papazafeiropoulos, "Downlink performance of massive MIMO under general channel aging conditions," in *Proc. IEEE Global Commun. Conf. (GLOBECOM)*, Dec. 2015, pp. 1–6.

[24] Y. Zou, P. Zetterberg, U. Gustavsson, T. Svensson, A. Zaidi, T. Kadur, W. Rave, and G. Fettweis, "Impact of major RF impairments on mm-wave communications using OFDM waveforms," in *Proc. IEEE Globecom Workshops (GC Wkshps)*, Dec. 2016, pp. 1–7.

[25] X. Gao, L. Dai, S. Han, C.-L. I, and R. W. Heath, Jr., "Energy-efficient hybrid analog and digital precoding for mmWave MIMO systems with large antenna arrays," *IEEE J. Sel. Areas Commun.*, vol. 34, no. 4, pp. 998–1009, Apr. 2016.

[26] O. E. Ayach, S. Rajagopal, S. Abu-Surra, Z. Pi, and R. W. Heath, Jr., "Spatially sparse precoding in millimeter wave MIMO systems," *IEEE Trans. Wireless Commun.*, vol. 13, no. 3, pp. 1499–1513, Mar. 2014.

[27] X. Yu, J.-C. Shen, J. Zhang, and K. B. Letaief, "Alternating minimization algorithms for hybrid precoding in millimeter wave MIMO systems," *IEEE J. Sel. Topics Signal Process.*, vol. 10, no. 3, pp. 485–500, Apr. 2016.

[28] Y. Li, S. He, C. Ma, S. Ma, C. Li, and L. Yang, "Channel characteristic and capacity analysis of millimeter wave MIMO beamforming system," in *Proc. IEEE 83rd Veh. Technol. Conf. (VTC Spring)*, May 2016, pp. 1–5.

[29] R. W. Heath, Jr., N. Gonzalez-Prelcic, S. Rangan, W. Roh, and A. M. Sayeed, "An overview of signal processing techniques for millimeter wave MIMO systems," *IEEE J. Sel. Topics Signal Process.*, vol. 10, no. 3, pp. 436–453, Apr. 2016.
[30] S. Han, C.-L. I, Z. Xu, and C. Rowell, "Large-scale antenna systems with hybrid analog and digital beamforming for millimeter wave 5G," *IEEE Commun. Mag.*, vol. 53, no. 1, pp. 186–194, Jan. 2015.
[31] J. S. Lu, D. Steinbach, P. Cabrol, and P. Pietraski "Modeling human blockers in millimeter wave radio links," *ZTE Commun.*, vol. 10, pp. 23–28, Dec. 2012.
[32] E. Bjornson, J. Hoydis, M. Kountouris, and M. Debbah, "Massive MIMO systems with non-ideal hardware: Energy efficiency, estimation, and capacity limits," *IEEE Trans. Inf. Theory*, vol. 60, no. 11, pp. 7112–7139, Nov. 2014.
[33] S. He, C. Qi, Y. Wu, and Y. Huang, "Energy-efficient transceiver design for hybrid sub-array architecture MIMO systems," *IEEE Access*, vol. 4, pp. 9895–9905, 2016.
[34] R. Mendez-Rial, C. Rusu, N. Gonzalez-Prelcic, A. Alkhateeb, and R. W. Heath, Jr., "Hybrid MIMO architectures for millimeter wave communications: Phase shifters or switches?" *IEEE Access*, vol. 4, pp. 247–267, 2016.
[35] N. Maletic, J. Gutierrez-Teran, and E. Grass, "Beamforming mmWave MIMO: Impact of nonideal hardware and channel state information," in *Proc. 26th Telecommun. Forum (TELFOR)*, Serbia, Belgrade, Nov. 2018, pp. 1–6.
[36] M. Wu, D. Wubben, A. Dekorsy, P. Baracca, V. Braun, and H. Halbauer, "Hardware impairments in millimeter wave communications using OFDM and SC-FDE," in *Proc. 20th Int. ITG Workshop Smart Antennas (WSA)*, Munich, Germany, Mar. 2016, pp. 1–8.
[37] C.-S. Choi, Y. Shoji, H. Harada, R. Funada, S. Kato, K. Maruhashi, I. Toyoda, and K. Takahashi, "RF impairment models for 60 GHz-band SYS/PHY simulation," NICT, NEC, NTT, and Panasonic, Yokosuka, Japan, Tech. Rep. 802.15-06-0477-01-003c, Nov. 2006.
[38] R. Gomes, Z. Al-Daher, A. Hammoudeh, K. Sobaihi, R. Caldeirinha, and T. Fernandes, "Performance and evaluation of OFDM and SC–FDE over an AWGN propagation channel under RF impairments using simulink at 60 GHz," in *Proc. Loughborough Antennas Propag. Conf. (LAPC)*, Loughborough, U.K., Nov. 2014, pp. 685–689.
[39] M. Lei, M. A. Rahman, I. Lakkis, C.-S. Sum, T. Baykas, J.-Y. Wang, R. Kimura, R. Funada, Y. Shoji, H. Harada, and S. Kato, "Hardware impairments on LDPC coded SC-FDE and OFDM in multi-Gbps WPAN (IEEE 802.15.3c)," in *Proc. IEEE Wireless Commun. Netw. Conf.*, Las Vegas, NV, USA, Mar. 2008, pp. 442–446.
[40] T. A. Thomas, H. C. Nguyen, G. R. MacCartney, and T. S. Rappaport, "3D mmWave channel model proposal," in *Proc. IEEE 80th Veh. Technol. Conf. (VTC-Fall)*, Vancouver, BC, Canada, Sep. 2014, pp. 1–6.
[41] T. Bai, A. Alkhateeb, and R. Heath, "Coverage and capacity of millimeter-wave cellular networks," *IEEE Commun. Mag.*, vol. 52, no. 9, pp. 70–77, Sep. 2014.
[42] Y. Wu, Y. Gu, and Z. Wang, "Channel estimation for mmWave MIMO with transmitter hardware impairments," *IEEE Commun. Lett.*, vol. 22, no. 2, pp. 320–323, Feb. 2018.
[43] S. Rangan, T. S. Rappaport, and E. Erkip, "Millimeter-wave cellular wireless networks: Potentials and challenges," *Proc. IEEE*, vol. 102, no. 3, pp. 366–385, Mar. 2014.
[44] A. Demir, A. Mehrotra, and J. Roychowdhury, "Phase noise in oscillators: A unifying theory and numerical methods for characterization," *IEEE Trans. Circuits Syst. I, Fundam. Theory Appl.*, vol. 47, no. 5, pp. 655–674, May 2000.
[45] T. A. Thomas, M. Cudak, and T. Kovarik, "Blind phase noise mitigation for a 72 GHz millimeter wave system," in *Proc. IEEE Int. Conf. Commun. (ICC)*, London, U.K., Jun. 2015, pp. 8–12.
[46] O. Kolawole, A. Papazafeiropoulos, and T. Ratnarajah, "Impact of hardware impairments on mmWave MIMO systems with hybrid precoding," in *Proc. IEEE Wireless Commun. Netw. Conf. (WCNC)*, Apr. 2018, pp. 1–6.
[47] S. Li, B. Su, L. Jin, M. Cai, and H. Wu, "Joint measure matrix and channel estimation for millimeter-wave massive MIMO with hybrid precoding," *EURASIP J. Wireless Commun. Netw.*, vol. 2019, no. 1, p. 293, Dec. 2019.
[48] V. Raghavan and A. M. Sayeed, "Sublinear capacity scaling laws for sparse MIMO channels," *IEEE Trans. Inf. Theory*, vol. 57, no. 1, pp. 345–364, Jan. 2011.
[49] L. Tomba, "On the effect of Wiener phase noise in OFDM systems," *IEEE Trans. Commun.*, vol. 46, no. 5, pp. 580–583, May 1998.
[50] P. Almers, S. Wyne, F. Tufvesson, and A. F. Molisch, "Effect of random walk phase noise on MIMO measurements," in *Proc. IEEE 61st Veh. Technol. Conf.*, May/Jun. 2005, pp. 141–145.
[51] T. Höhne and V. Ranki, "Phase noise in beamforming," *IEEE Trans. Wireless Commun.*, vol. 9, no. 12, pp. 1696–1705, Dec. 2010.
[52] A. Taparugssanagorn and J. Ylitalo, "Characteristics of short-term phase noise of MIMO channel sounding and its effect on capacity estimation," *IEEE Trans. Instrum. Meas.*, vol. 58, no. 1, pp. 196–201, Jan. 2009.
[53] Y. Wang, J. Yang, W. Yin, and Y. Zhang, "A new alternating minimization algorithm for total variation image reconstruction," *SIAM J. Imag. Sci.*, vol. 1, no. 3, pp. 248–272, Jan. 2008.
[54] T. F. Chan and C. K. Wong, "Convergence of the alternating minimization algorithm for blind deconvolution," *Linear Algebra Appl.*, vol. 316, nos. 1–3, pp. 259–285, Sep. 2000.
[55] P. Jain, P. Netrapalli, and S. Sanghavi, "Low-rank matrix completion using alternating minimization," in *Proc. 45th Annu. ACM Symp. Symp. Theory Comput. (STOC)*, Palo Alto, CA, USA, 2013, pp. 665–674.
[56] H. Kim and H. Park, "Nonnegative matrix factorization based on alternating nonnegativity constrained least squares and active set method," *SIAM J. Matrix Anal. Appl.*, vol. 30, no. 2, pp. 713–730, Jan. 2008.
[57] J. Hu, X. Liu, Z.-W. Wen, and Y.-X. Yuan, "A brief introduction to manifold optimization," *J. Oper. Res. Soc. China*, vol. 8, no. 2, pp. 199–248, Jun. 2020.
[58] Y. Ma and Y. Fu, *Manifold Learning Theory and Applications*. Boca Raton, FL, USA: CRC Press, 2012.
[59] J. Lee, *Introduction to Smooth Manifolds*. Berlin, Germany: Springer, 2012.
[60] Y. Shi, J. Zhang, and K. B. Letaief, "Low-rank matrix completion via Riemannian pursuit for topological interference management," in *Proc. IEEE Int. Symp. Inf. Theory (ISIT)*, Hong Kong, Jun. 2015, pp. 1831–1835.
[61] P.-A. Absil, R. Mahony, and R. Sepulchre, *Optimization Algorithms on Matrix Manifolds*. Princeton, NJ, USA: Princeton Univ. Press, 2009.
[62] N. Boumal, B. Mishra, P.-A. Absil, and R. Sepulchre, "Manopt, a MATLAB toolbox for optimization on manifolds," *J. Mach. Learn. Res.*, vol. 15, pp. 1455–1459, Aug. 2014.
[63] D. P. Bertsekas, *Nonlinear Programming*. Nashua, NH, USA: Athena Scientific, 1999.
[64] I. Ziskind and M. Wax, "Maximum likelihood localization of multiple sources by alternating projection," *IEEE Trans. Acoust., Speech, Signal Process.*, vol. 36, no. 10, pp. 1553–1560, Oct. 1988.
[65] D. L. Donoho and Y. Tsaig, "Fast solution of ℓ_1-norm minimization problems when the solution may be sparse," *IEEE Trans. Inf. Theory*, vol. 54, no. 11, pp. 4789–4812, Nov. 2008.
[66] S. Suyama, H. Suzuki, K. Fukawa, and J. Izumi, "Iterative receiver employing phase noise compensation and channel estimation for millimeter-wave OFDM systems," *IEEE J. Sel. Areas Commun.*, vol. 27, no. 8, pp. 1358–1366, Oct. 2009.
[67] X. Chen, H. Wang, W. Fan, Y. Zou, A. Wolfgang, T. Svensson, and J. Luo, "Phase noise effect on MIMO-OFDM systems with common and independent oscillators," *Wireless Commun. Mobile Comput.*, vol. 2017, pp. 1–12, Nov. 2017.
[68] S. M. Kay, *Fundamentals of Statistical Signal Processing: Estimation Theory*. Englewood Cliffs, NJ, USA: Prentice-Hall, 1993.
[69] H. Yu and M.-C.-F. Chang, "A 1-V 1.25-GS/S 8-Bit self-calibrated flash ADC in 90-nm digital CMOS," *IEEE Trans. Circuits Syst. II, Exp. Briefs*, vol. 55, no. 7, pp. 668–672, Jul. 2008.
[70] S. Saponara and B. Neri, "Integrated 60 GHz antenna, LNA and fast ADC architecture for embedded systems with wireless Gbit connectivity," *J. Circuits, Syst. Comput.*, vol. 21, no. 5, Aug. 2012, Art. no. 1250047.
[71] M. Miyahara, I. Mano, M. Nakayama, K. Okada, and A. Matsuzawa, "A 2.2GS/s 7b 27.4 mW time-based folding-flash ADC with resistively averaged voltage-to-time amplifiers," in *Proc. IEEE Int. Solid-State Circuits Conf. Dig. Tech. Papers (ISSCC)*, Feb. 2014, pp. 388–389.
[72] E. Alpman, H. Lakdawala, L. R. Carley, and K. Soumyanath, "A 1.1 V 50 mW 2.5GS/s 7b time-interleaved C-2C SAR ADC in 45 nm LP digital CMOS," in *IEEE Int. Solid-State Circuits Conf. (ISSCC) Dig. Tech. Papers*, Feb. 2009, pp. 76–77.
[73] A. S. Y. Poon and M. Taghivand, "Supporting and enabling circuits for antenna arrays in wireless communications," *Proc. IEEE*, vol. 100, no. 7, pp. 2207–2218, Jul. 2012.
[74] M. Uzunkol and G. M. Rebeiz, "A 65 GHz LNA/Phase shifter with 4.3 dB NF using 45 nm CMOS SOI," *IEEE Microw. Wireless Compon. Lett.*, vol. 22, no. 10, pp. 530–532, Oct. 2012.

[75] M. R. Akdeniz, Y. Liu, M. K. Samimi, S. Sun, S. Rangan, T. S. Rappaport, and E. Erkip, "Millimeter wave channel modeling and cellular capacity evaluation," *IEEE J. Sel. Areas Commun.*, vol. 32, no. 6, pp. 1164–1179, Jun. 2014.
[76] H. Yan, S. Ramesh, T. Gallagher, C. Ling, and D. Cabric, "Performance, power, and area design trade-offs in millimeter-wave transmitter beamforming architectures," *IEEE Circuits Syst. Mag.*, vol. 19, no. 2, pp. 33–58, 2nd Quart., 2019.
[77] A. Es-saqy, M. Abata, M. Mehdi, S. Mazer, M. Fattah, M. El Bekkali, and C. Algani, "28 GHz balanced pHEMT VCO with low phase noise and high output power performance for 5G mm-wave systems," *Int. J. Electr. Comput. Eng.*, vol. 10, no. 5, pp. 4623–4630, 2020.

OSAMA S. FARAGALLAH received the B.Sc. (Hons.), M.Sc., and Ph.D. degrees in computer science and engineering from Menoufia University, Menouf, Egypt, in 1997, 2002, and 2007, respectively. He was a Demonstrator and an Assistant Lecturer with the Department of Computer Science and Engineering, Faculty of Electronic Engineering, Menoufia University, from 1997 to 2002 and 2002 to 2007, respectively, where he has been a Teaching Staff Member since 2007 and a Professor since 2018. In 2015, he joined the Department of Information Technology, College of Computers and Information Technology, Taif University, Al-Hawiya, Saudi Arabia. He is a coauthor of about 200 papers in international journals and conference proceedings, and two textbooks. His current research interests include network security, cryptography, the Internet security, multimedia security, image encryption, watermarking, steganography, data hiding, medical image processing, remote sensing, chaos theory, and mobile communications.

HALA S. EL-SAYED received the B.Sc. (Hons.), M.Sc., and Ph.D. degrees in electrical engineering from Menoufia University, Shebin El-Kom, Egypt, in 2000, 2004, and 2010, respectively. She was a Demonstrator and an Assistant Lecturer with the Department of Electrical Engineering, Faculty of Engineering, Menoufia University, from 2002 to 2004 and 2004 to 2010, respectively, where she has been a Teaching Staff Member since 2010 and is currently an Assistant Professor. She is a coauthor of about 50 papers in international journals and conference proceedings, and one textbook. Her research interests include database security, network security, data hiding, image encryption, wireless sensor networks, secure building automation systems, and biometrics.

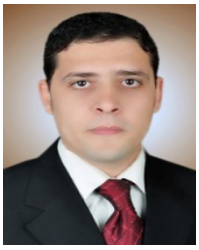

MOHAMED G. EL-MASHED received the B.Sc. (Hons.), M.Sc., and Ph.D. degrees from the Faculty of Electronic Engineering, Menoufia University, Egypt, in 2008, 2012, and 2015, respectively. He joined the Teaching Staff of the Department of Electronics and Electrical Communications, Faculty of Electronic Engineering, Menoufia University. His research interests include ultra-wide band (UWB) radar applications, radar signal processing and imaging, MIMO radar systems, SAR imaging techniques, digital signal processing, advanced communication systems, WiMAX, LTE, LTE-A, massive MIMO systems, and FPGA implementation in communication systems.